UNITED NATIONS EDUCATIONAL, SCIENTIFIC AND CULTURAL ORGANIZATION
INTERNATIONAL ATOMIC ENERGY AGENCY
INTERNATIONAL CENTRE FOR THEORETICAL PHYSICS

SMR/917 - 28

SECOND WORKSHOP ON SCIENCE AND TECHNOLOGY OF THIN FILMS

(11 - 29 March 1996)

" Thin-film deposition "

presented by:

D.L. SMITH
Xerox Palo Alto Research Center
3333 Coyote Hill Road
CA 94304 Palo Alto
U.S.A.

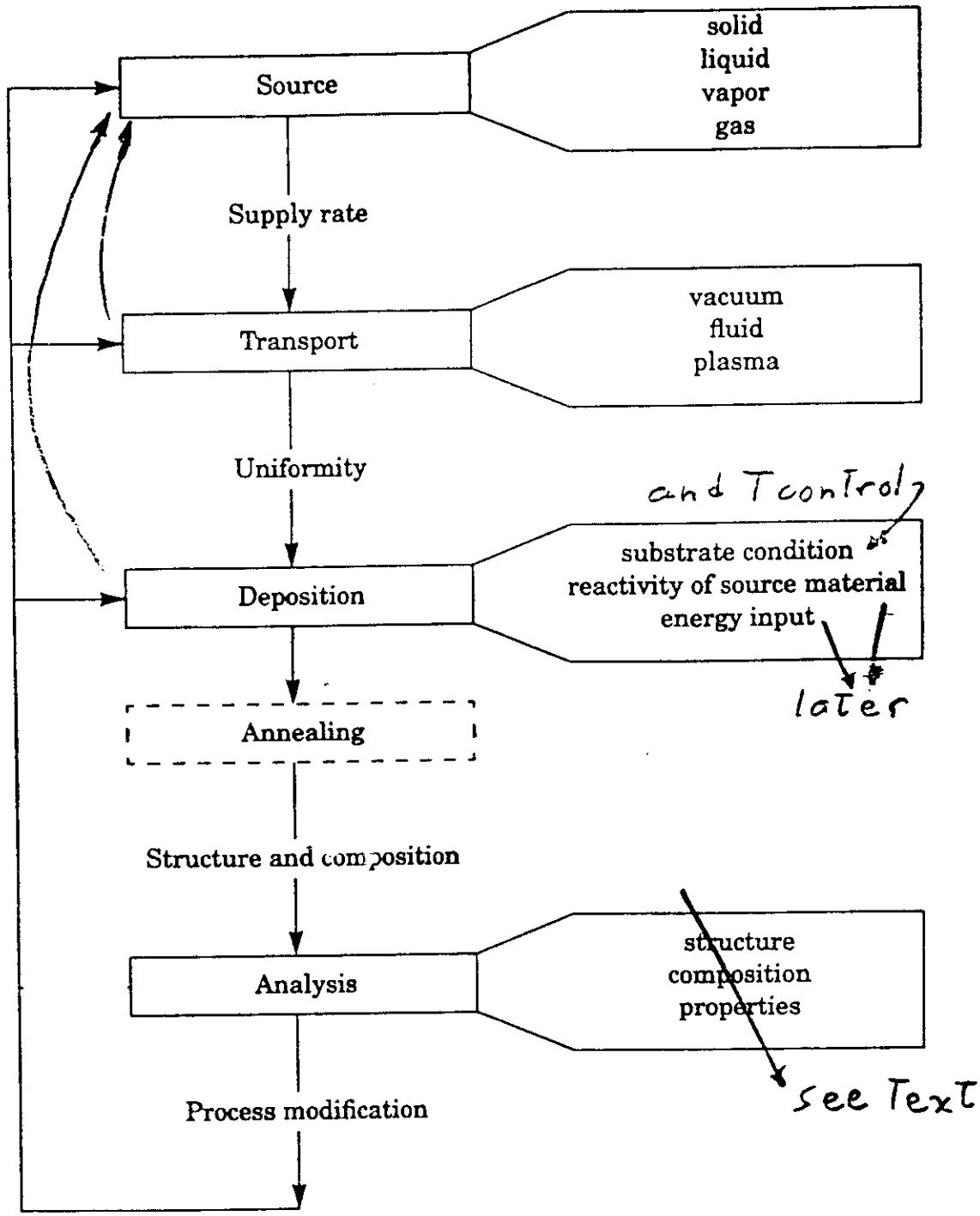
Source
solid
liquid
vapor
gas
Supply rate
Transport
vacuum
fluid
plasma
Uniformity
and T control
Deposition
substrate condition
reactivity of source material
energy input
later
Annealing
Structure and composition
Analysis
structure
composition
properties
see Text
Process modification

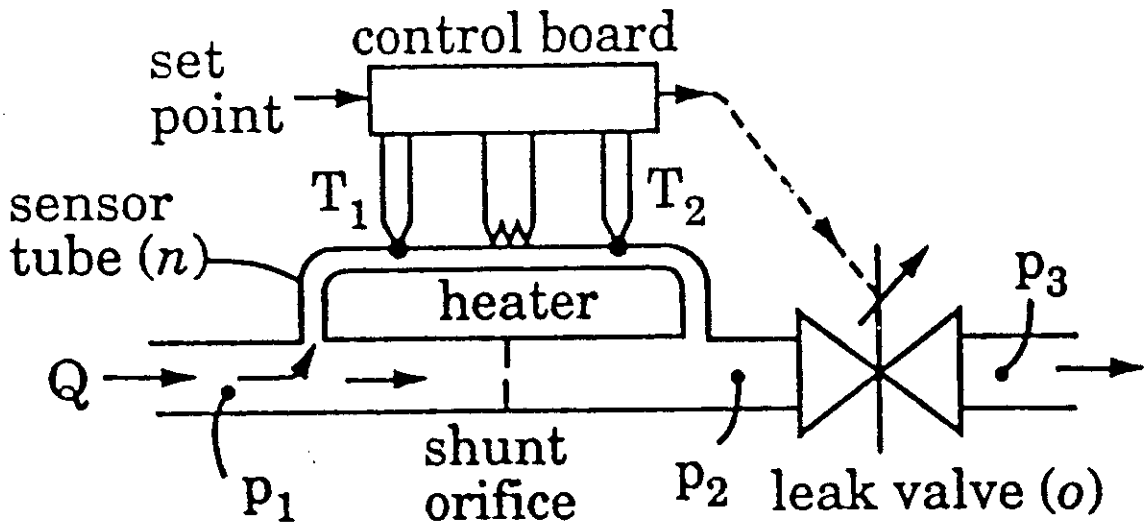
control board
set
point
sensor
tube (n)
T1
T2
heater
Q
p3
p1
shunt
orifice
p2
leak valve (o)

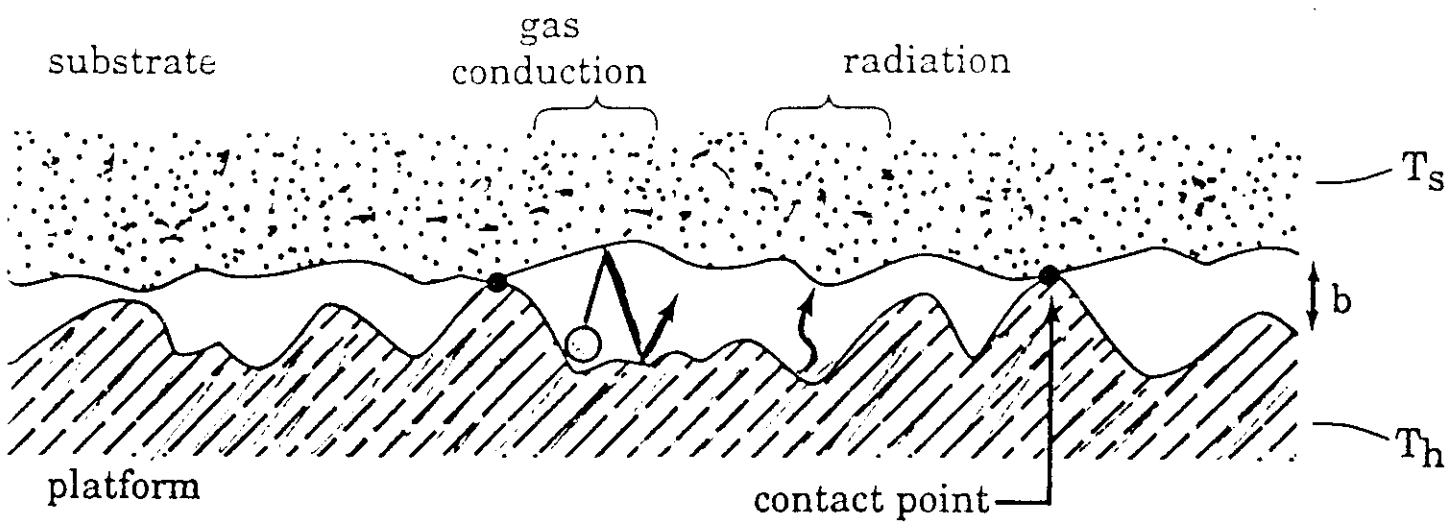
substrate
gas
conduction
radiation
T_s
b
T_h
platform
contact point

$\frac{1}{2} mv^2 = 0.04$ eV/mc at room T
$= 0.3$ eV at 2000 K

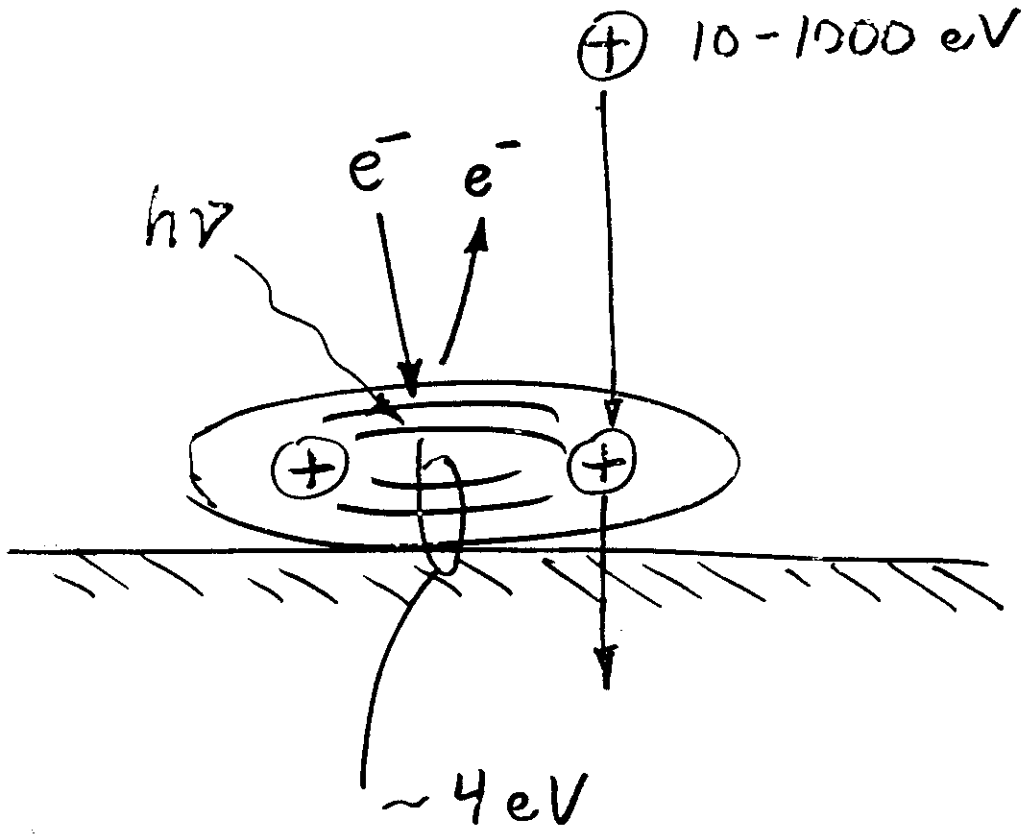

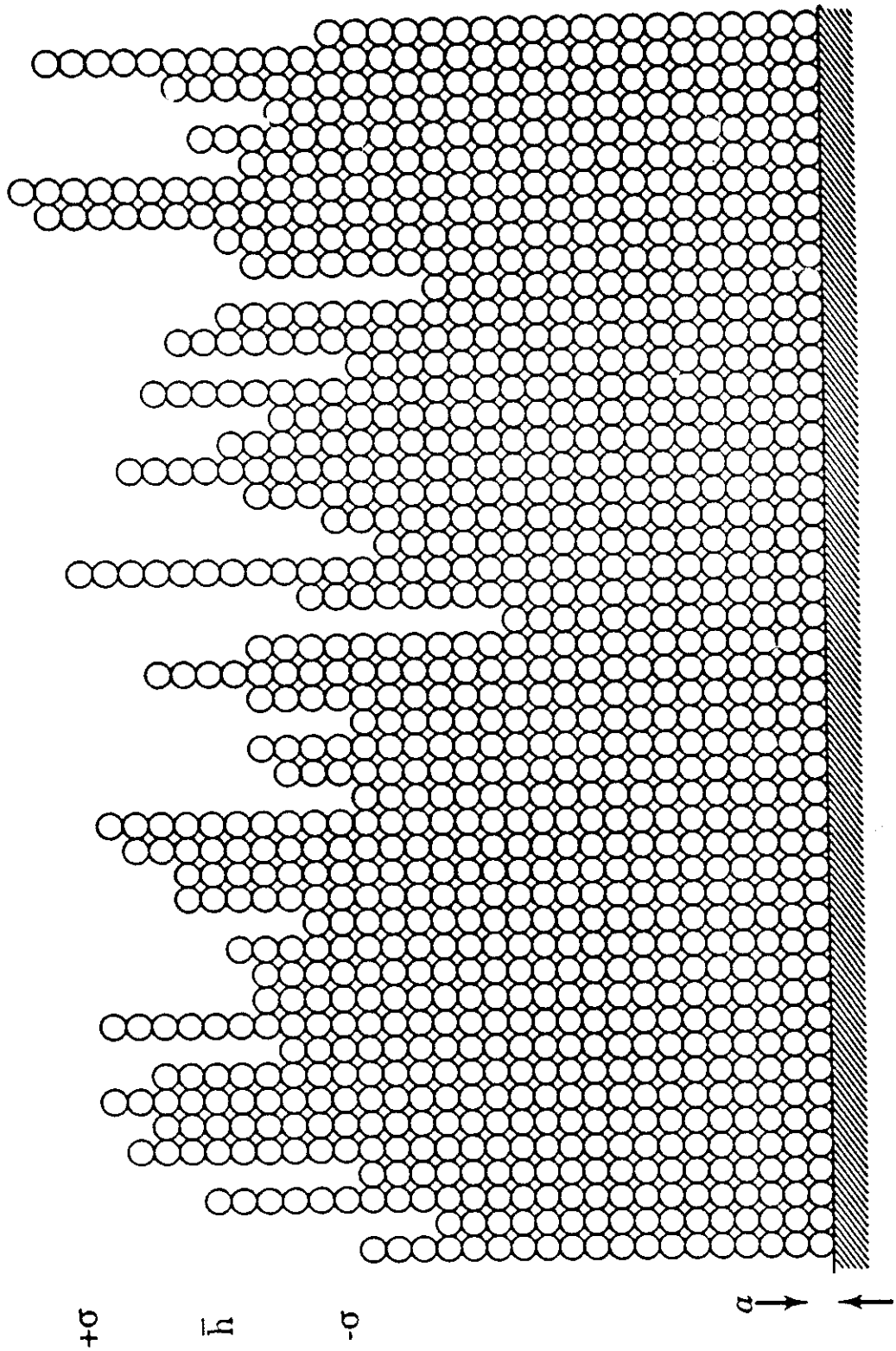
a
a-
h
a+

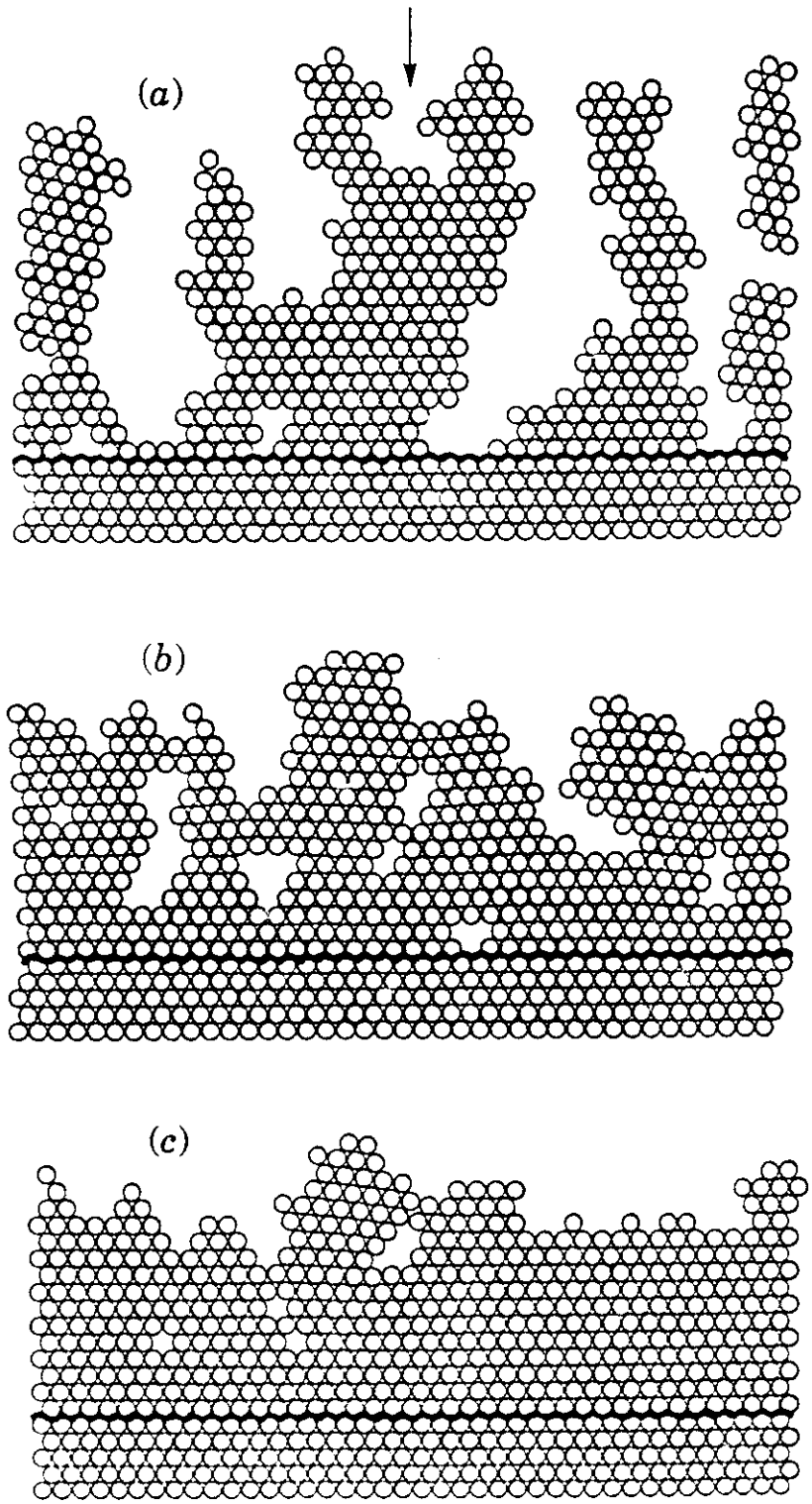
(a)
(b)
(c)

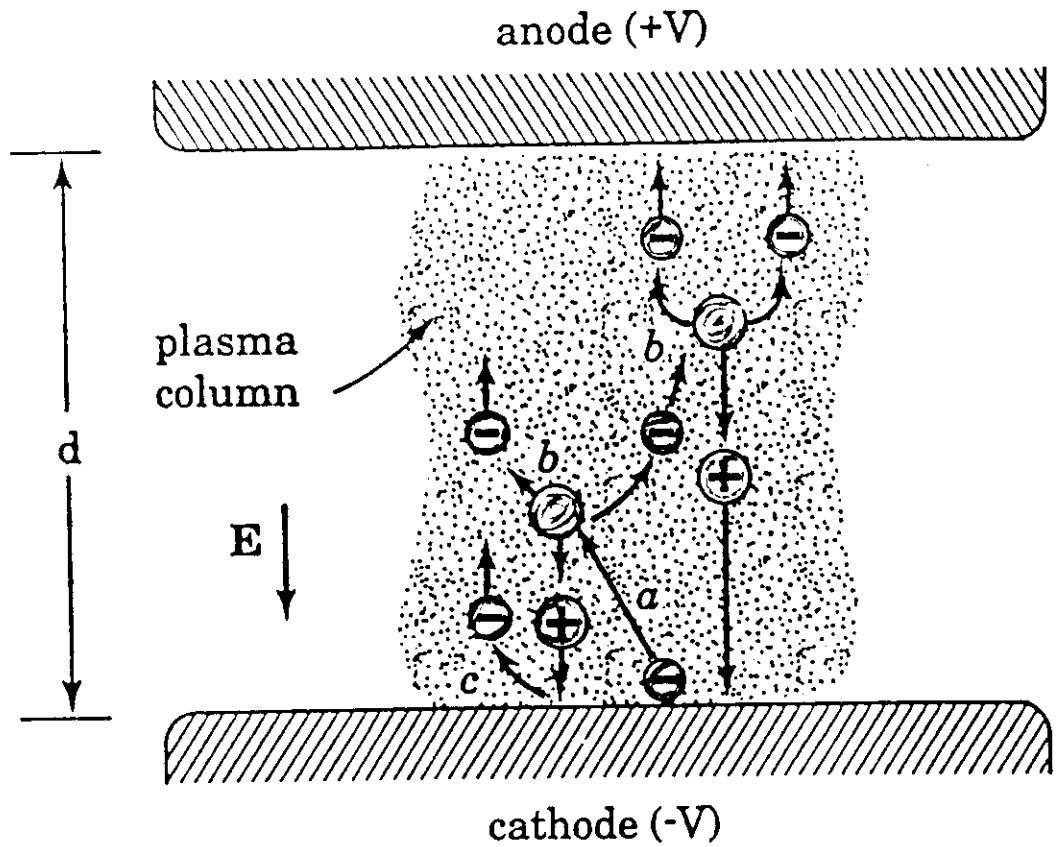
anode (+V)
plasma
column
d
E
b
b
a
c
cathode (-V)

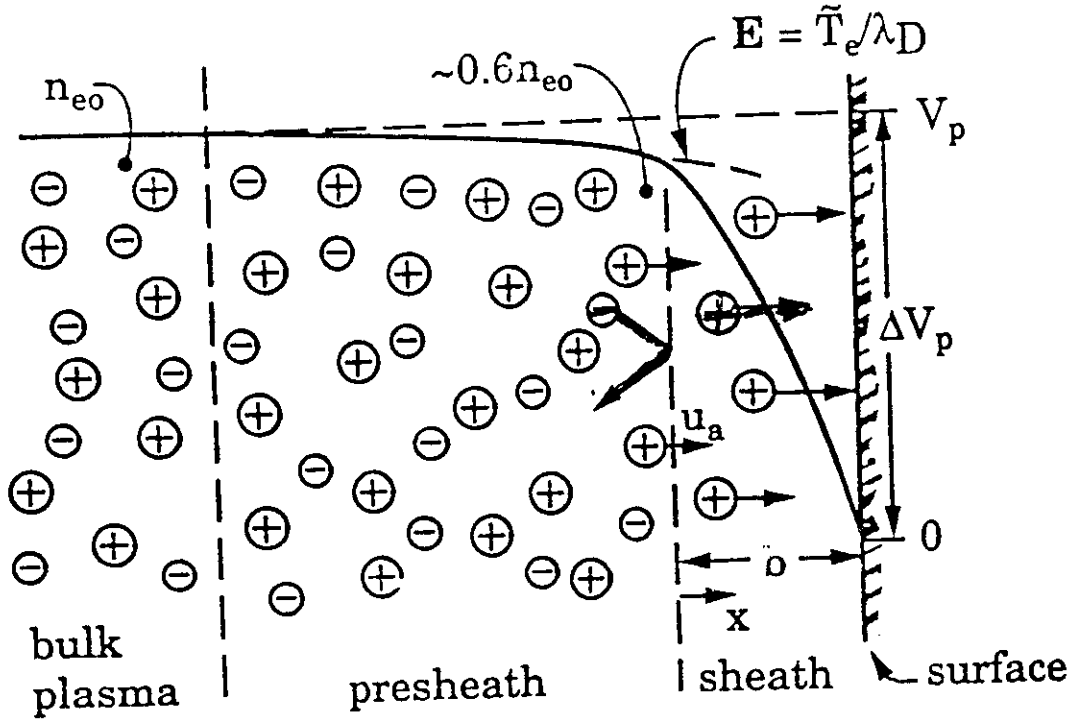
E = T̃e/λD
~0.6neo
neo
Vp
ΔVp
ua
0
o
x
bulk
plasma
presheath
sheath
surface

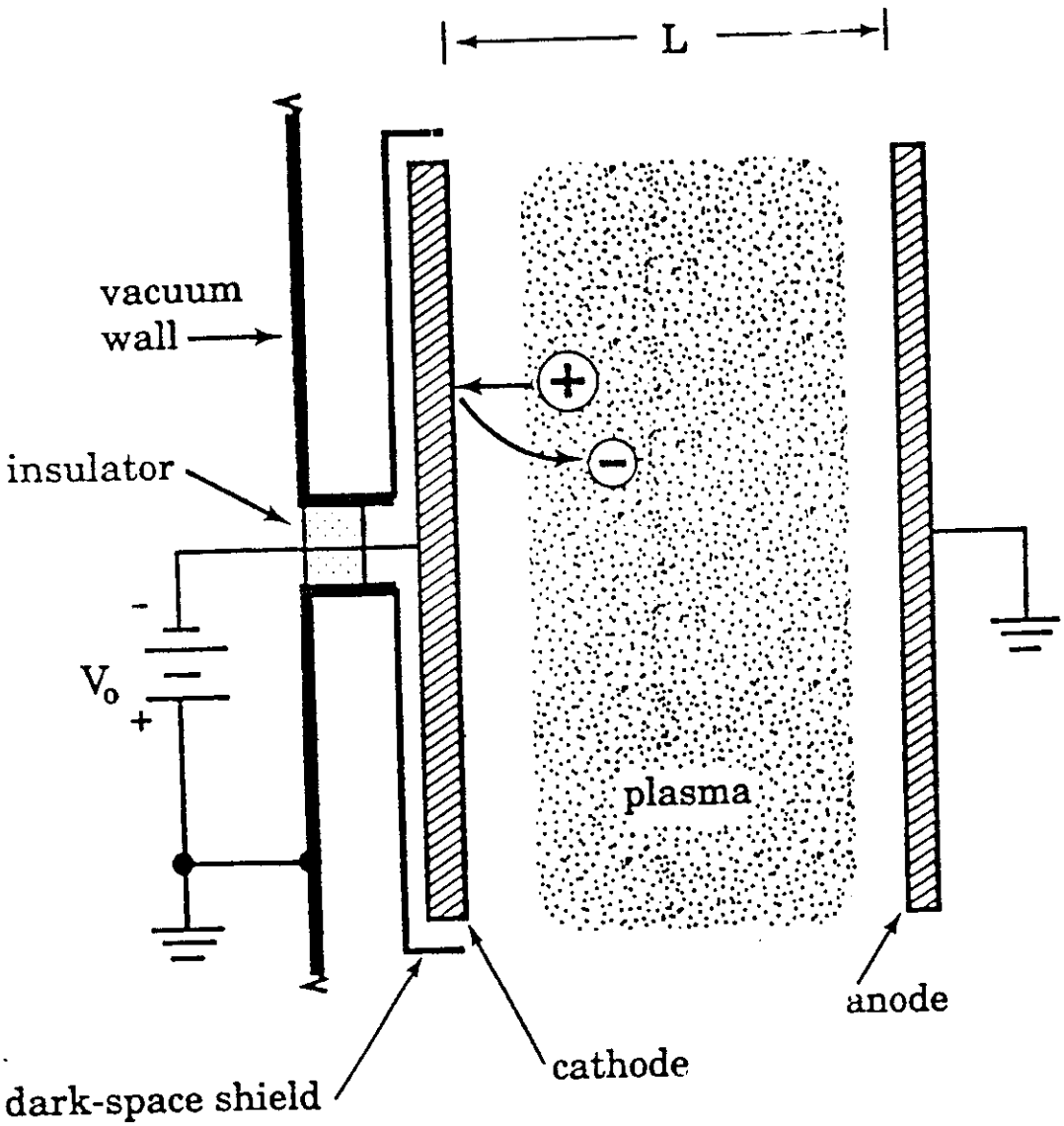
L
vacuum wall
insulator
-
V_o
+
plasma
anode
cathode
dark-space shield

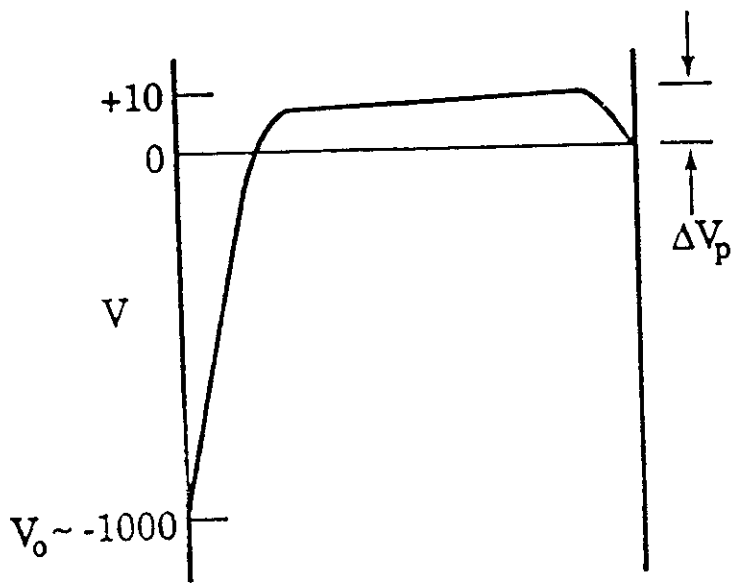
+10
0
V
V_o ~ -1000
ΔV_p

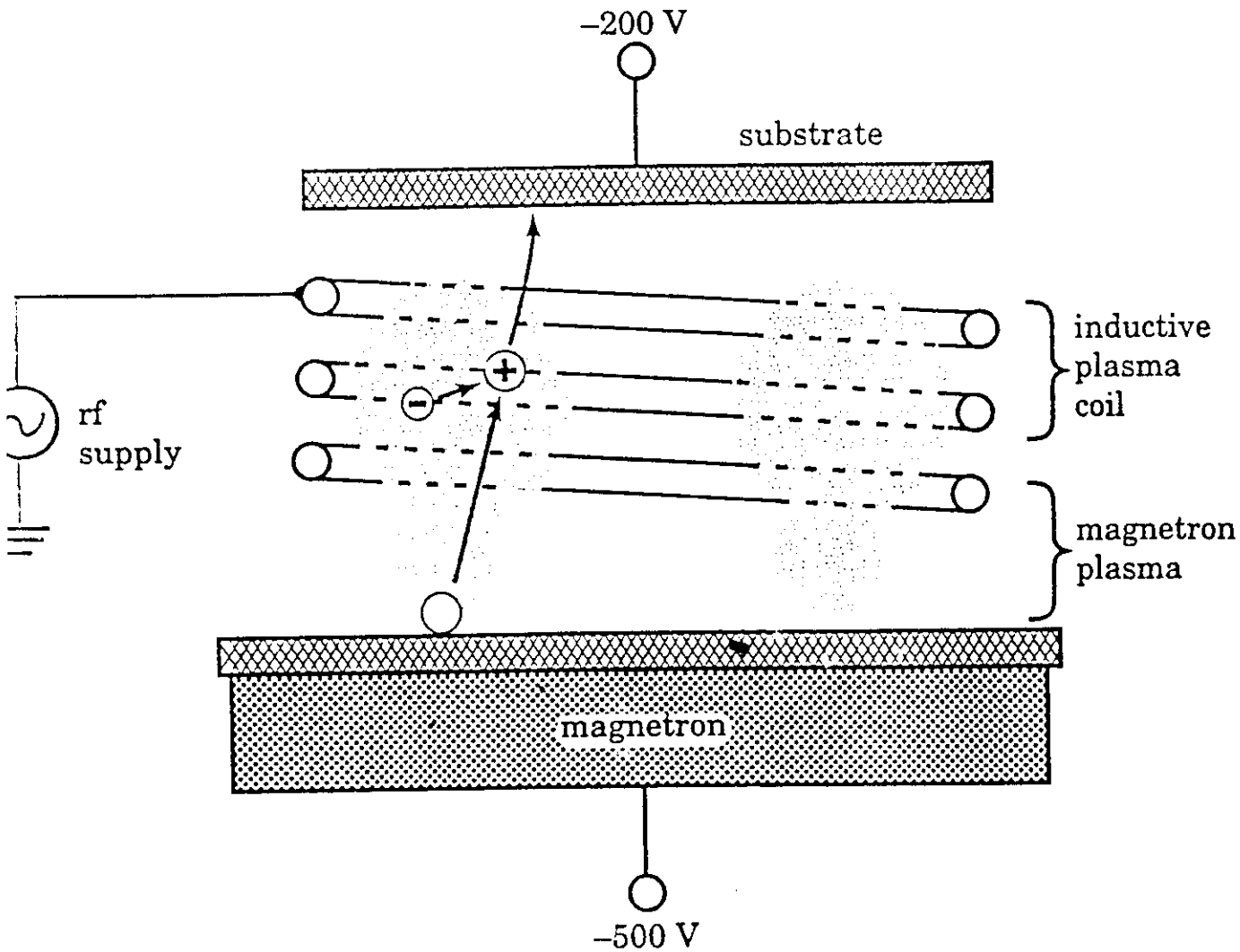
–200 V
substrate
inductive
plasma
coil
rf
supply
magnetron
plasma
magnetron
–500 V

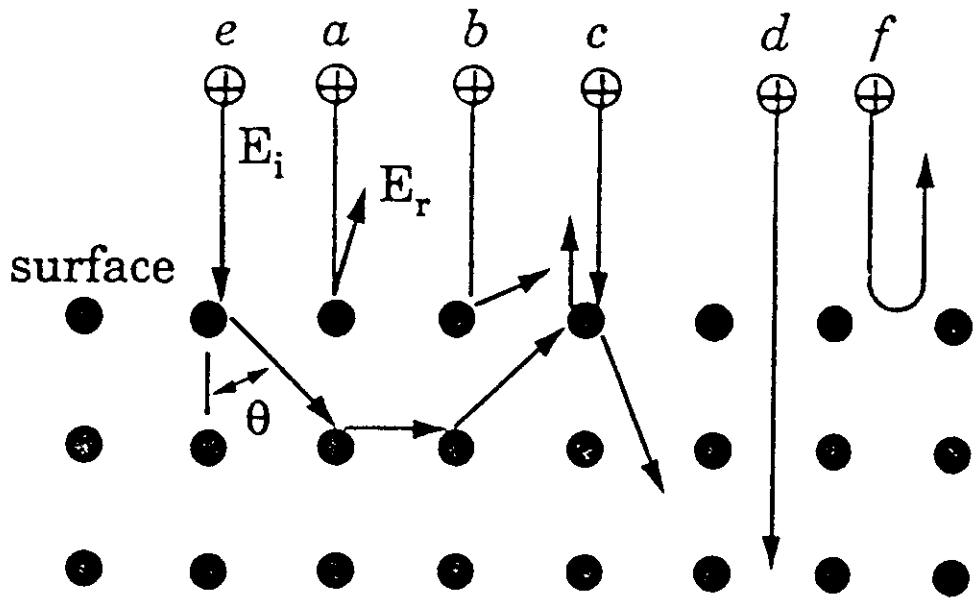
e
a
b
c
d
f
E_i
E_r
surface
θ

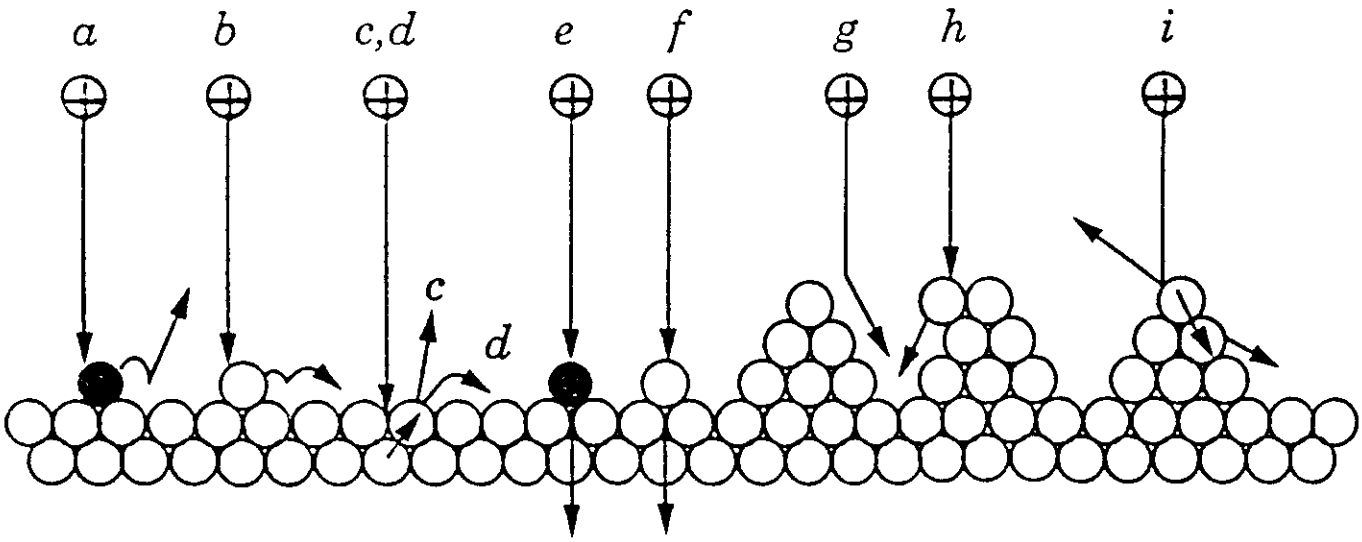
a
b
c,d
e
f
g
h
i
c
d

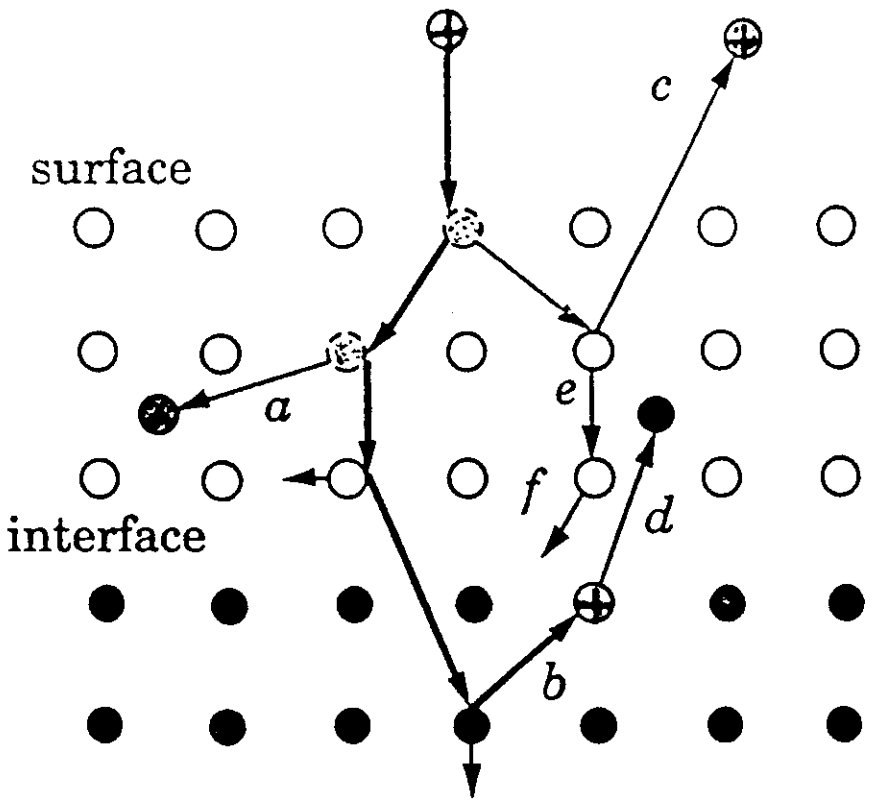
surface
interface
a
b
c
d
e
f

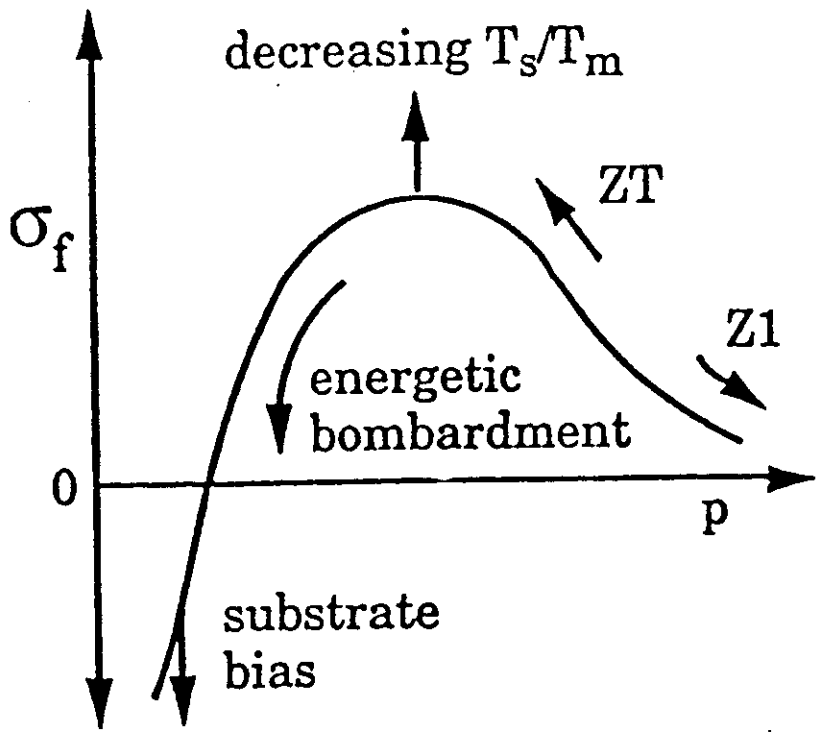
decreasing T_s/T_m
ZT
σ_f
Z1
energetic
bombardment
0
p
substrate
bias

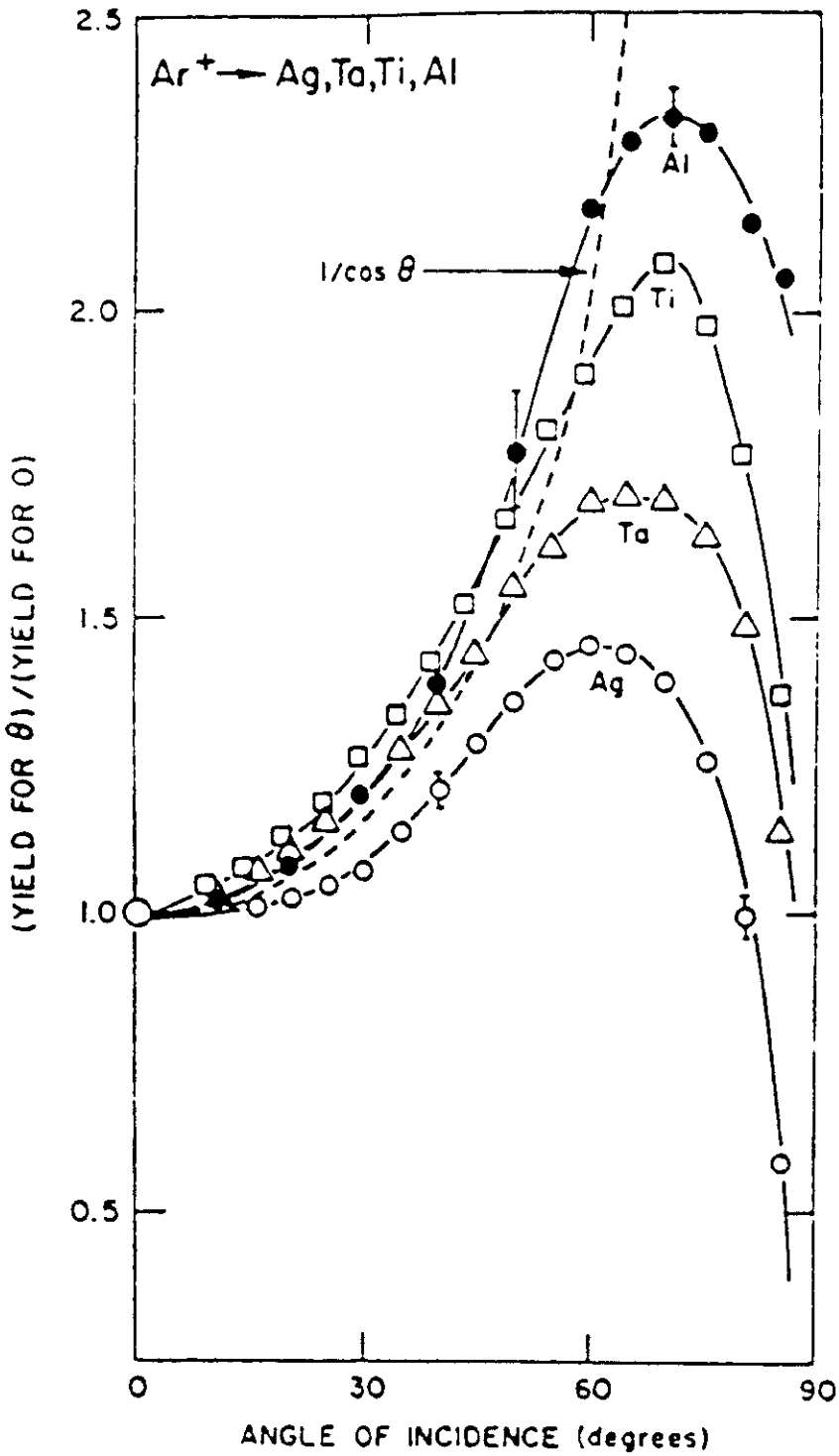
Ar+ → Ag,Ta,Ti,Al
1/cos θ
Al
Ti
Ta
Ag
2.5
2.0
1.5
1.0
0.5
0
30
60
90
(YIELD FOR θ)/(YIELD FOR 0)
ANGLE OF INCIDENCE (degrees)

2µm

$$G = \overbrace{U + pV}^{H\ (enthalpy)} - TS \rightarrow \text{min. at equilibrium at constant } p$$

also $R_+ = R_-$

$$k = k_+ n \quad \text{for } 1^{ST} \text{ order}$$

$$k = \nu_+ e^{-E_a/RT}$$

For $aA + bB \rightleftharpoons cC + dD$,

$$K = \frac{P_C^c P_D^d}{P_A^a P_B^b} = \frac{k_+}{k_-} = \frac{\nu_+}{\nu_-} e^{-(E_{a+} - E_{a-})/RT}$$

$$= e^{-\Delta_r G^\circ/RT} = e^{\Delta S^\circ/R} e^{-\Delta_r H^\circ/RT}$$

(P° = 1 bar)

examples:

$$WF_6(g) + \tfrac{3}{2} SiO_2(c) \rightleftharpoons \tfrac{3}{2} SiF_4(g) + \tfrac{3}{2} O_2(g)$$

$$\Delta_r G = +420 \text{ kJ/mole}$$

$$WF_6(g) + \tfrac{3}{2} Si(c) \rightleftharpoons \tfrac{3}{2} SiF_4(g) + W(c)$$

$$\Delta_r G = -707 \text{ kJ/mole}$$

GaAs MOCVD: $C(a) + 2H_2(g) \rightleftharpoons CH_4(g)$

(H_2: diluent)

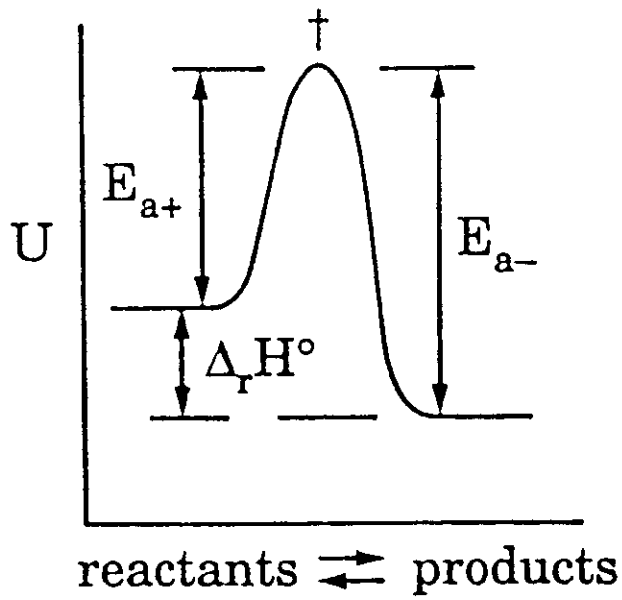
†
U
E_{a+}
E_{a-}
$\Delta_r H°$
reactants ⇌ products

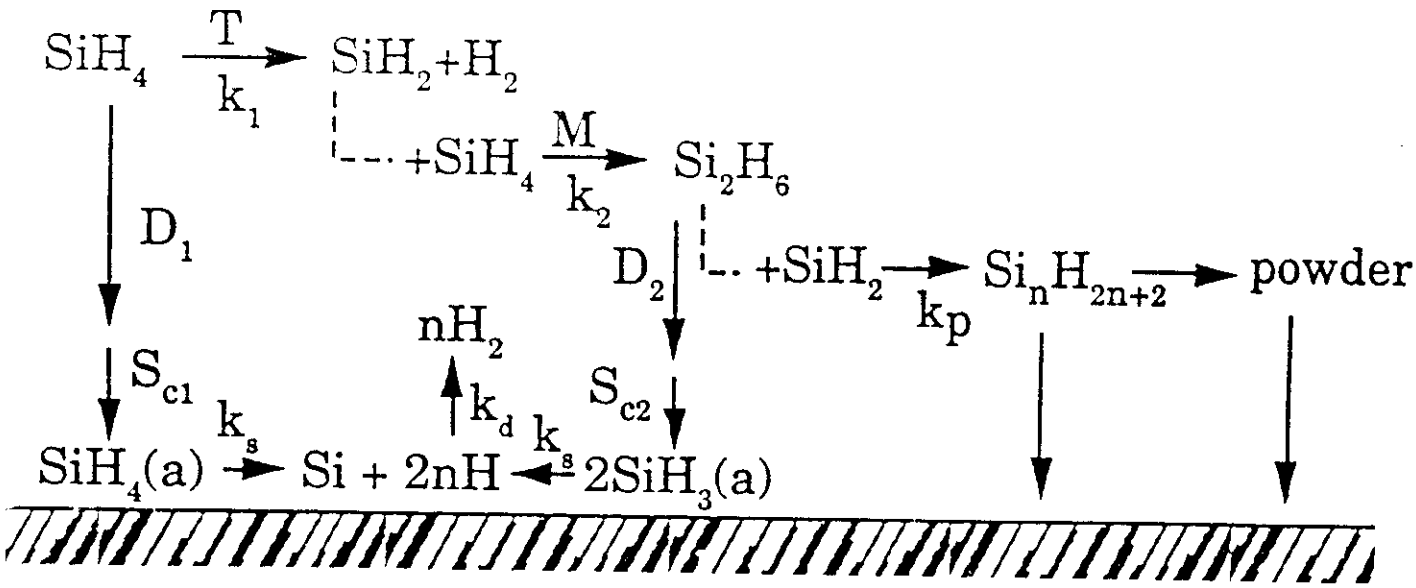
SiH4
T
k1
SiH2+H2
+SiH4
M
k2
Si2H6
D1
D2
+SiH2
kp
SinH2n+2
powder
nH2
Sc1
kd
Sc2
ks
ks
SiH4(a)
Si + 2nH
2SiH3(a)

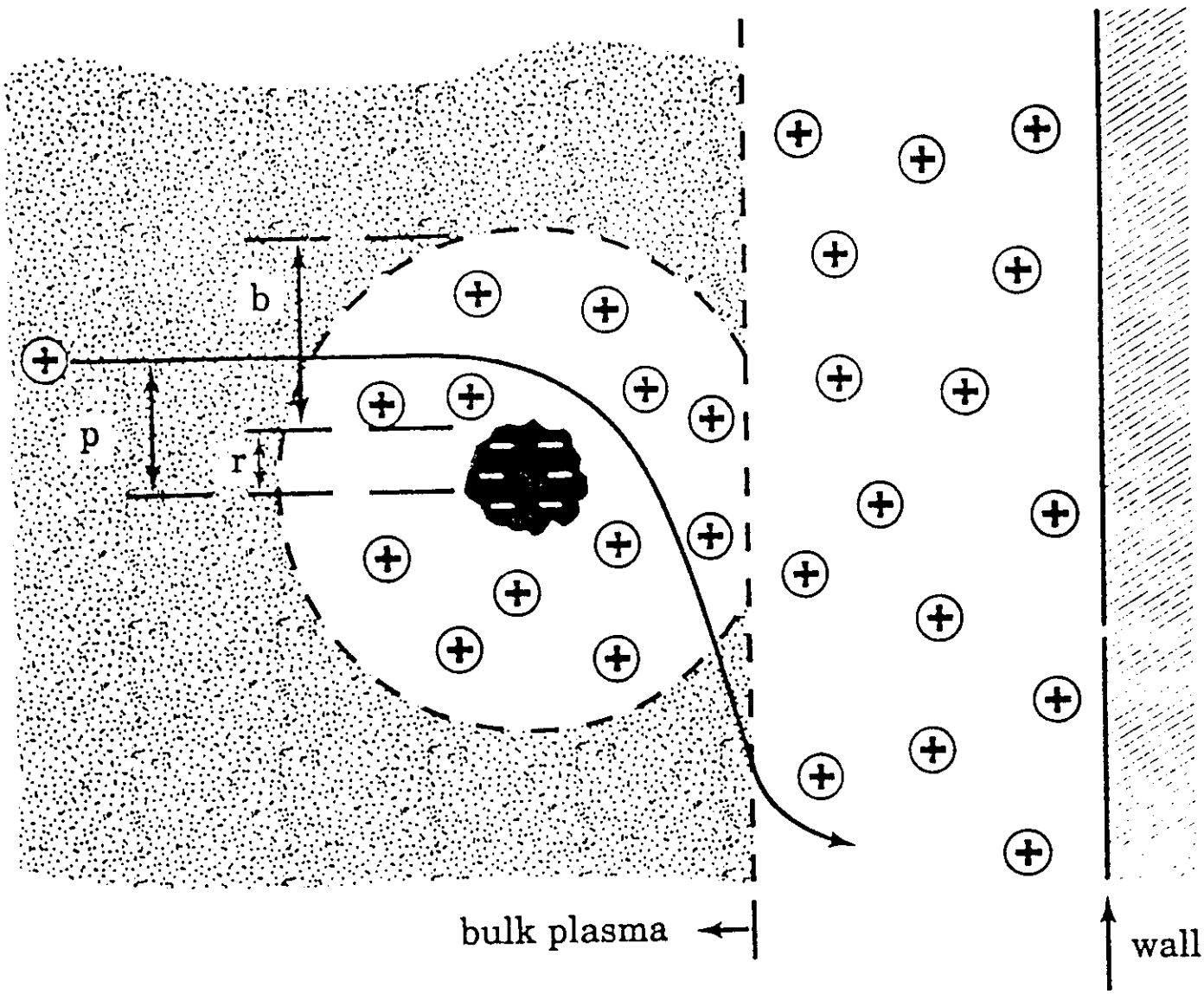
b
p
r
bulk plasma
wall

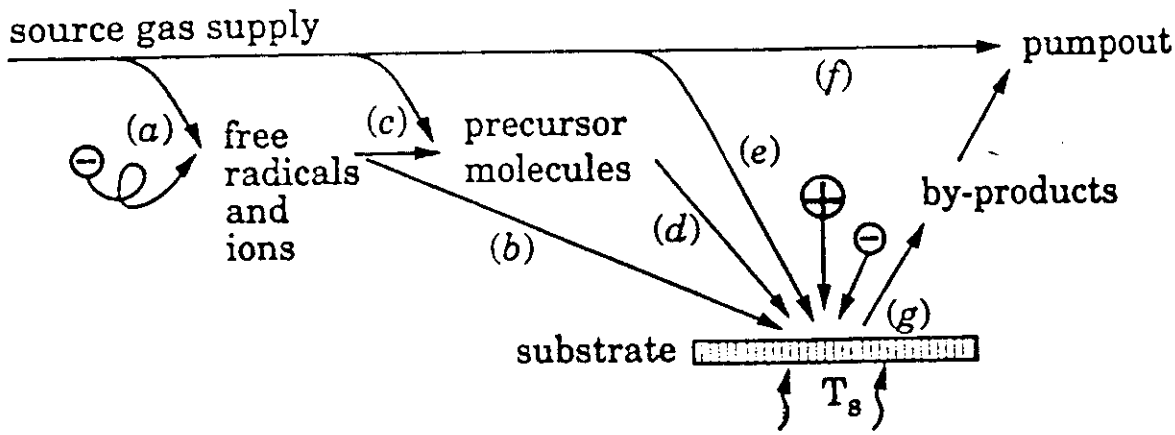
source gas supply
pumpout
(f)
(a)
free
radicals
and
ions
(c)
precursor
molecules
(e)
by-products
(d)
(b)
(g)
substrate
T_s

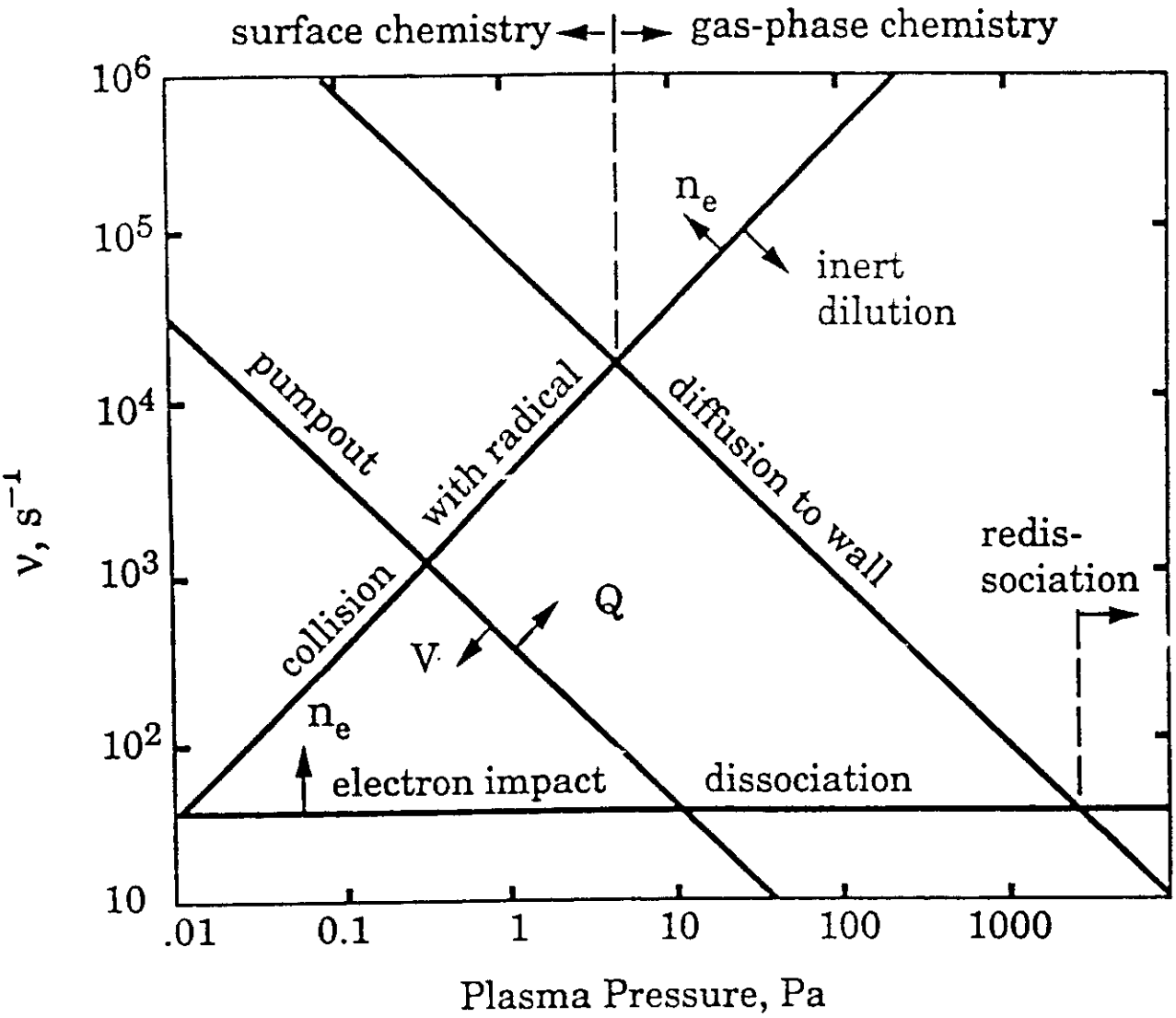
surface chemistry
gas-phase chemistry
10^6
10^5
10^4
10^3
10^2
10
n_e
inert
dilution
pumpout
with radical
diffusion to wall
redis-
sociation
collision
Q
V
n_e
electron impact
dissociation
.01
0.1
1
10
100
1000
Plasma Pressure, Pa
ν, s^{-1}

Ammonia Process Analysis

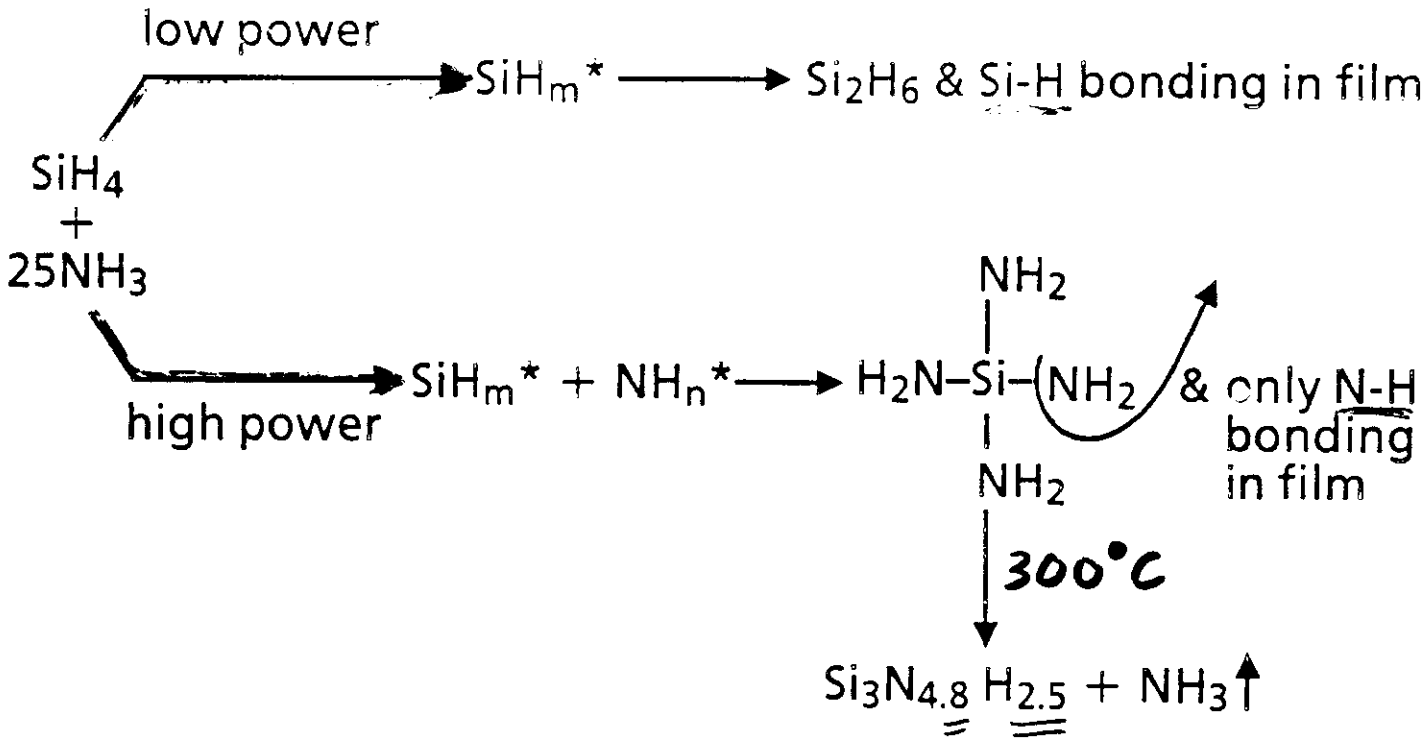

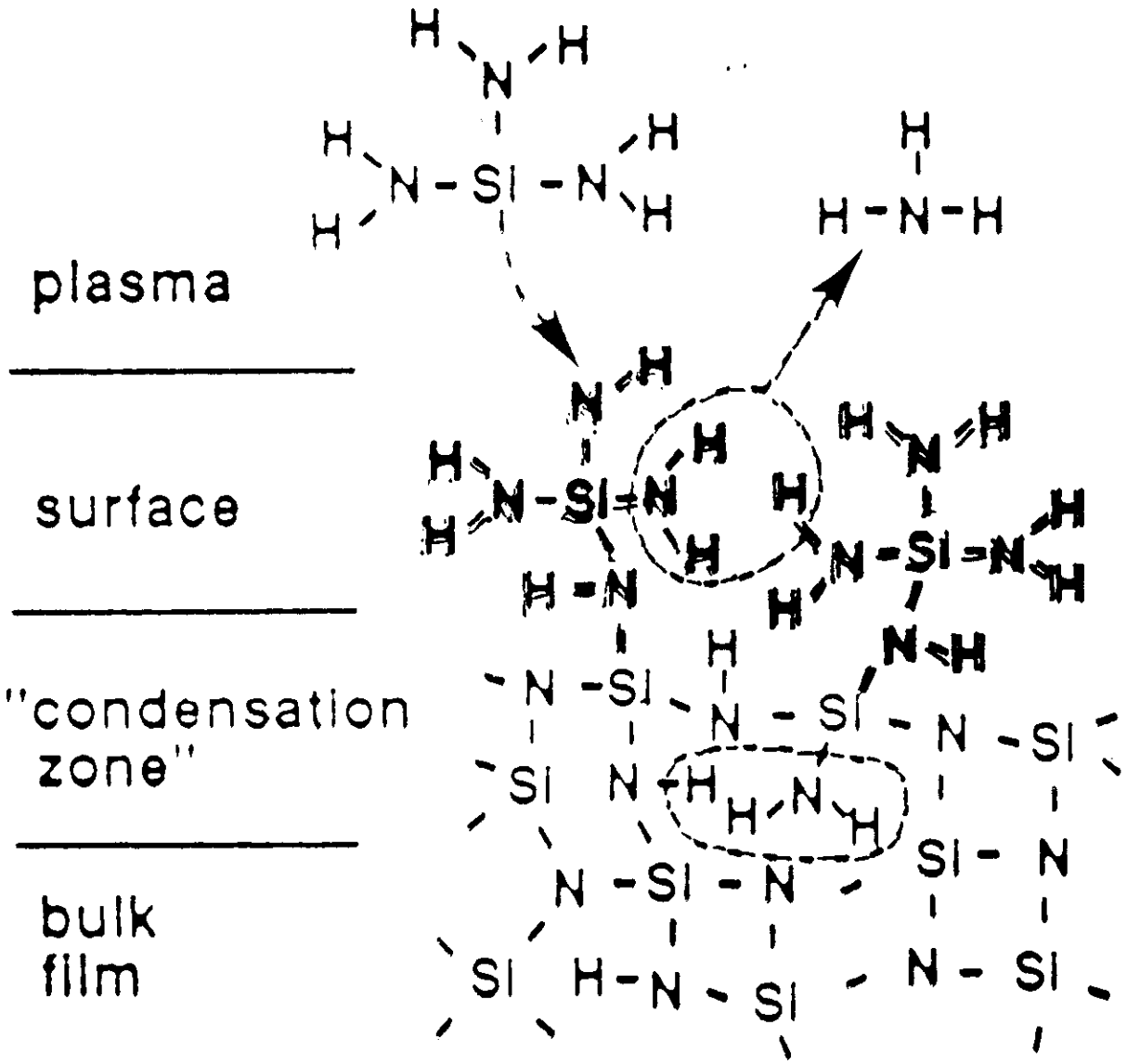
plasma
surface
"condensation zone"
bulk film

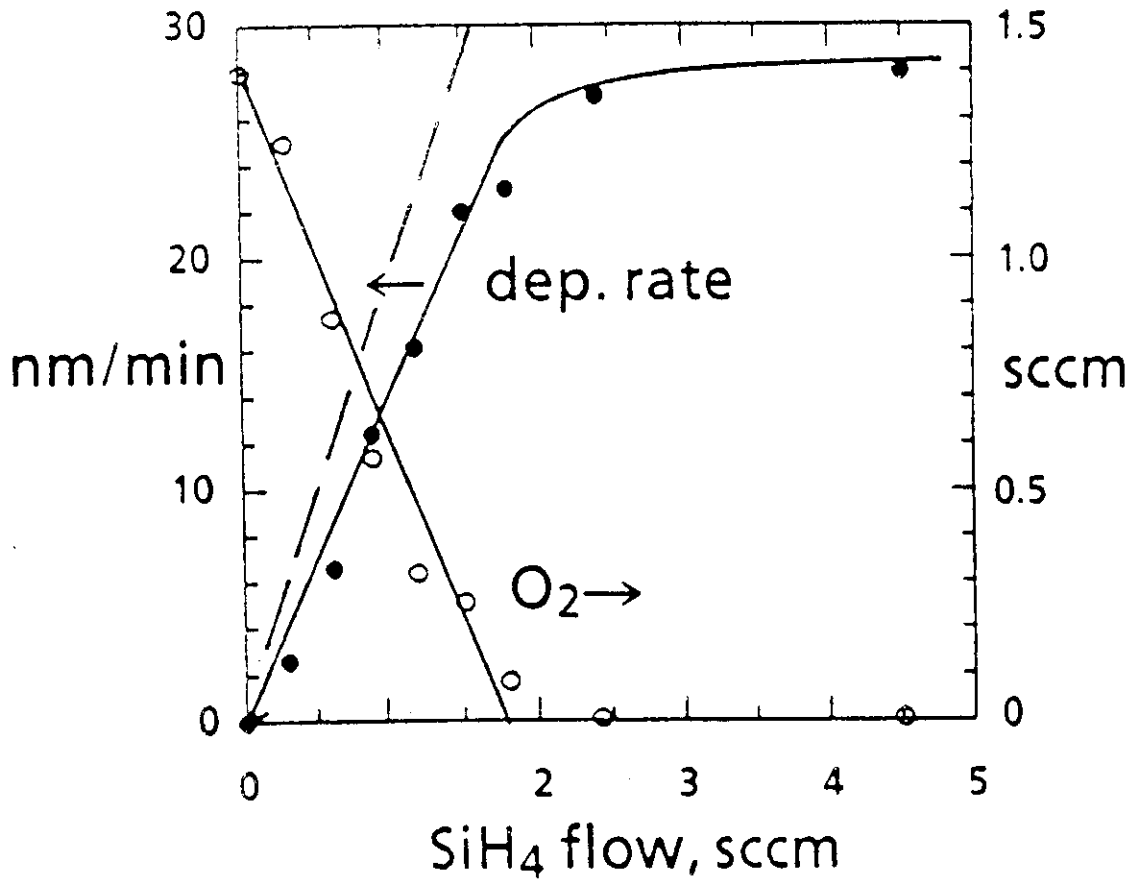

EIL

PARC

Controlling the plasma chemistry of silicon nitride and oxide deposition from silane

Donald L. Smith
Xerox Palo Alto Research Center, 3333 Coyote Hill Road, Palo Alto, California 94304

(Received 5 November 1992; accepted 4 January 1993)

We have studied the chemistry of glow discharge plasma-enhanced chemical vapor deposition (PECVD) by using vibrating quartz crystal deposition rate monitoring at 200–300 °C and line-of-sight mass spectrometry of orifice-sampled reactive neutral species. In the deposition of dielectric films from silane plus a large excess of oxidant (NH_3, N_2, or N_2O), the key process factor is the ratio of plasma power to silane supply rate. When enough of the oxidant is activated by the plasma, it completely converts the silane to films which have no excess Si and no Si–H bonding. The critical ratio can be detected by the disappearance of Si_2H_6 byproduct or by the presence of excess activated oxidant. Nitride deposited from N_2 is electrically leaky due to porous microstructure even when deposited using excess activated oxidant. Conversely, nitride deposited from NH_3 is nonporous, and when deposited using excess activated oxidant it has a surprisingly low electron trapping rate which is at least as low as that achievable in PECVD oxide. Deposition using N_2 involves no formation of gas-phase precursor molecules; but using NH_3, $^{\bullet}Si(NH_2)_3$, and $Si(NH_2)_4$ were the dominant precursors. SiO_2 deposition from N_2O involved a minor contribution from $Si(OH)_4$. High reactant partial pressure or excess rf power can lead to particle formation and deposition rate loss, especially in SiO_2 deposition, due to gas-phase reaction among precursors. Partial pressure reduction either by He dilution or by total pressure reduction suppressed these problems with equal effectiveness in SiO_2 deposition. No other effects of He could be detected either in the plasma chemistry or in the bulk film trapping rate.

I. INTRODUCTION

Plasma-enhanced chemical vapor deposition (PECVD) is a widely used process for depositing thin films at low substrate temperature. In the low-pressure glow discharge plasma, energy in the form of fast electrons takes the place of thermal energy in activating the desired CVD reactions, by dissociating the chemical vapor molecules to produce highly reactive free radicals. However, further details about the deposition chemistry usually are not known, and so process conditions are adjusted empirically based on measured film properties. Because the fast electrons can break any chemical bond, it is generally believed that the plasma will contain a broad array of species too complex for analysis. Fortunately, we have found the situation to be less complex in cases we have examined. This appears to be due to the dominance of thermochemical reactions, even though electron-impact dissociation is the *initiating* process. In a series of studies, our group has analyzed the chemistry of dielectric film deposition from silane-based (SiH_4) plasmas, including "silicon nitride" (actually SiN_xH_y) deposited using NH_3[1] or N_2,[2] and SiO_2 using N_2O.[3] We have then shown that the electron trapping rate, which is a particularly sensitive measure of dielectric film quality, is greatly reduced when plasma chemistry is controlled in SiN_xH_y deposition.[4,5] Indeed, the rate is lower than that of the best PECVD SiO_2.[5] In SiO_2 deposition, both the plasma chemistry[3] and the bulk trapping rate[6] were found to be the same whether or not He dilution was employed, despite much speculation in the literature about the role of He in plasma chemistry and although the use of He may be improving Si substrate *interface* quality.[7]

The PECVD process may be viewed as a sequence of events: (1) application of the process variables, principally gas mixture, pressure, electrical power, ion bombardment energy, and substrate temperature; (2) gas phase chemistry occurring within the plasma; (3) deposition and surface chemistry; (4) development of film composition and structure; and (5) resulting film properties. Most of the large literature on PECVD discusses the relationship between (1) and (5), and many useful, reliable deposition recipes have been developed by iteration around this loop. However, a deeper understanding of the PECVD process requires examination of the intermediate events. There has been considerable work on (4), but very little on (2) and (3). Examination of (3) is hampered by interference of the plasma with surface analysis. We chose to examine (2), along with (4) and (5). In the following sections, we discuss our analytical techniques and then compare and contrast the deposition chemistry and film properties for the three gas mixtures cited above, namely SiH_4 plus NH_3, N_2, or N_2O. We also propose some simple procedures for "tuning" a given PECVD reactor to maximize dielectric film quality, given this understanding of the plasma chemistry.

II. PLASMA ANALYTICAL TECHNIQUES

Film deposition and plasma analysis were carried out simultaneously in a parallel plate, 13 MHz rf reactor of conventional design which has been described previously.[1] It had a 180 cm^2 rf electrode spaced 3 cm from a larger

 0734-2101/93/11(4)/1843/8/$1.00

26

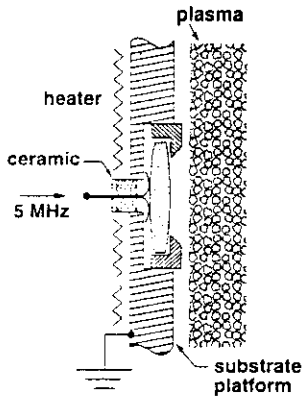

FIG. 1. Quartz crystal mount for stabilization at elevated temperature and for avoiding *rf* interference from the plasma.

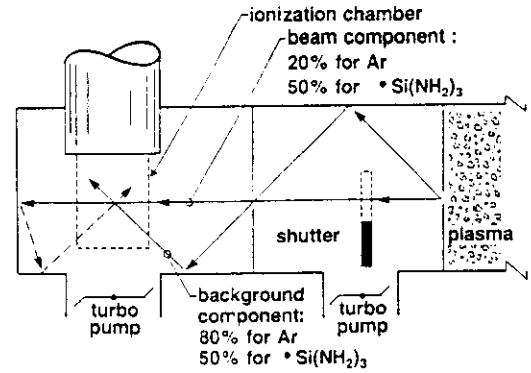

FIG. 2. System for line-of-sight sampling of plasma neutral species into a mass spectrometer. Relative values of direct and scattered signal components are shown for typical gaseous and depositing species: Ar and $^{\bullet}Si(NH_2)_3$, respectively.

grounded electrode. Substrates and analytical sampling were both positioned on the grounded electrode, which was also heated to give typical substrate temperatures of a few hundred °C. The analytical tools were quartz crystal deposition rate monitoring and line-of-sight mass spectrometry through a sampling orifice. Both techniques measure the species which are also arriving at the adjacent substrate surface and are therefore particularly relevant to the study of the deposition process. That is, we learn what species are arriving at the surface and how much material deposits.

Quartz crystal deposition monitors are generally operated at room temperature because they are deliberately cut at the crystallographic angle which gives a near-zero temperature coefficient of resonant frequency, $\Delta f/\Delta T$, at this temperature. However, film deposition rate is temperature dependent in PECVD, so it is important to monitor at the actual deposition temperature. Such operation results in a higher $\Delta f/\Delta T$ and proportionally more interference of this f shift with the f shift due to film deposition. Nevertheless, a crystal mounted within the substrate platform as shown in Fig. 1 is sufficiently f stable when good proportional/integral control is used to stabilize substrate platform temperature. An f transient is encountered due to a change in heat balance when the plasma is turned on, but this dies out within 10 s or so. This mount also avoids plasma rf interference with the 5 MHz quartz excitation and sensing signals. Above 350 °C or so, resonance could not be sustained.

The mass spectrometric sampling system shown in Fig. 2 is set up for the detection of neutral species. A parallel-plate glow-discharge plasma typically attains a plasma density of 10^{10} cm^{-3}, plasma density being the electron (and ion) concentration. By comparison, the concentration of free radicals is of the order of 10% of the molecular concentration, and the latter is 2.4×10^{16} cm^{-3} at 100 Pa and room temperature. Thus, the reactive neutral species exceed the ionic species by over 10^5, and film deposition is dominated by neutral species, although ion bombardment can certainly modify film structure. Figure 2 shows the line-of-sight molecular beam path for these plasma species from the sampling orifice in the substrate platform to the ionization chamber of the mass spectrometer. This direct beam path is the key to being able to detect the depositing species, which cannot be seen in conventional mass spectrometry using leak valve plumbing. The sampling orifices are small in diameter (0.25 mm) so as not to distort the electric field of the plasma sheath; the orifice plate is thin (0.1 mm) to minimize species loss to the orifice sidewalls; and an array of seven orifices is used to boost signal level. Two stages of differential pumping are used to reduce the signal of the scattered sample component relative to the beam component, and a vibrating-reed chopper synchronized with a gated pulse counter is used to distinguish beam ion counts from background counts. Most of the scattered component of the signal at the mass spectrometer comes from effusion through the collimating orifice located between the chopper and the ionization chamber, and this component does not get chopped. The signal component coming from beam species scattered in the mass spectrometer chamber, shown by the dashed line in Fig. 2, does get chopped, but it is very small at the ionization chamber compared to the direct beam signal. Chopped beam sampling not only separates out the species which come directly from the plasma without wall collision, but it also identifies which species are the depositing ones, because those have lower scattered signal components as a result of wall deposition. This effect is shown in Fig. 2 for an Ar beam versus a beam of the triaminosilane radical, $^{\bullet}Si(NH_2)_3$, which turned out to be the key depositing species in SiN_xH_y deposition from NH_3.[1]

There are several possible interferences in the identification of species by mass spectrometry, and their avoidance required special techniques in the work discussed here. For example, neutral species to be analyzed must first be ionized, usually by electron impact, and this ionization can be dissociative; thus, $N_2 + e \rightarrow N^+ + {}^{\bullet}N$. This N^+ interferes with the detection of $^{\bullet}N$ generated in the plasma. However, the electron energy threshold for $^{\bullet}N$ ionization (the ion appearance potential) is only 15 eV, while that of dissociative ionization is 24 eV,[8] an amount which is higher by about the N–N bond strength. Thus, the interference can be avoided by operating the electron source below 24 eV.[7] In the cases of NH_3 and N_2O, the appearance poten-

tial differences are not large enough to remove the dissociative component. Nevertheless, the degree of plasma dissociation of N_2O into $N_2 + {}^{\bullet}O$ can be monitored by the amount of O_2 formed in $^{\bullet}O$ recombination on the walls.[3] There, the $^{16}O^{18}O$ isotope was used to avoid interference from $^{14}N^{18}O$ at mass 32. The last technique is triple quadrupole mass spectrometry (TQMS), which can resolve compositional ambiguities at a given mass number. For example, the key peak seen in SiN_xH_y deposition from $NH_3 + SiH_4$ occurred at mass 76, which could be from either $^{\bullet}Si(NH_2)_3$ or $^{\bullet}N(SiH_3)_2$, both likely candidates. TQMS can "dissect" this ion by secondary cracking upon impact with Ar injected into the second quadrupole, and in this case the resulting "daughter" ion had mass 59, which is 76 minus NH_3.[1] The $^{\bullet}Si(NH_2)_3$ can decompose to give NH_3, but the $^{\bullet}N(SiH_3)_2$ would give SiH_4; thus, the ambiguity is resolved.

III. DEPOSITION CHEMISTRY

In this section, we discuss significant similarities and differences which we observed in the plasma chemistry of dielectric deposition from SiH_4 plus NH_3,[1] N_2,[2] and N_2O.[3] The three processes behave similarly in several ways, and these characteristics can be used to "tune" the plasma chemistry for desired film properties. In all cases, an active oxidant which can react with the $^{\bullet}SiH_n$ radicals must be produced by electron-impact dissociation in the plasma: $NH_3 \rightarrow {}^{\bullet}NH_{n<3}$, $N_2 \rightarrow {}^{\bullet}N$, and $N_2O \rightarrow {}^{\bullet}O$. The amount of the oxidant radical produced increases with plasma power, and to produce good dielectric film there must be an excess of it beyond the amount needed to consume all of the $^{\bullet}SiH_n$. We will see below how to determine the critical power level. At this power level, the SiH_4 will have become mostly dissociated into $^{\bullet}SiH_n$, because it does so at extremely low power densities. In our reactor, half of the SiH_4 was dissociated with only 1 W of power at 13 Pa and at the flow rate of 0.3 sccm used for SiO_2 deposition. Now, at such a low power level, insufficient active oxidant is present even though the oxidant source gas is present in large excess. Then, the $^{\bullet}SiH_n$ mostly reacts with itself to form Si_2H_n byproducts, and a smaller fraction deposits on the walls as amorphous Si (a-Si). This results in low deposition rates and in Si-rich films which are electrically leaky. The unactivated source gases do not react with the $^{\bullet}SiH_n$, and instead act as inert diluents. The higher the SiH_4 flow rate, the more power is needed to produce enough active oxidant to consume all of the $^{\bullet}SiH_n$, so the ratio

$$F = (\text{rf power, W})/(SiH_4 \text{ flow rate, sccm}) \qquad (1)$$

is a convenient empirical measure of the oxidation state of the plasma chemistry.

Figure 3(top) shows the characteristic behavior of the Si_2H_6 (disilane) byproduct signal and the film deposition rate for all three processes as the rf power is increased at a fixed SiH_4 flow rate. As power is raised, more of the $^{\bullet}SiH_n$ becomes oxidized (meaning also "nitrided") and deposited as dielectric film, and less of it appears as Si_2H_6. At the critical ratio, F_c, Si_2H_6 disappears completely, meaning orders of magnitude of attenuation. Also, deposition rate levels out, because all of the SiH_4 source gas has been oxidized. For power above F_c, excess oxidant is present, and fully oxidized films with good dielectric properties are produced. The value of F_c is not expected to vary much with deposition area, since both the power and the SiH_4 flow required should scale with area, neglecting edge losses. F_c does increase with the difficulty of dissociating the particular oxidant source gas. It is also likely to vary somewhat with electrode spacing and with rf frequency, because the steady-state dissociated gas fraction is a balance between its rate of generation by electron impact in the plasma and its rate of loss, which is partly by reaction on the walls. For our reactor, F_c was about 3 W/sccm for N_2O, 7 for NH_3, and 30 for N_2. Thus, N-rich SiN_xH_y can be made even from N_2 as long as sufficient power is applied. Of course, the oxidant source gas flow rate must be sufficient to produce enough active oxidant when a reasonable fraction of it, say 10%, has been dissociated. Thus, for example, the minimum amount of N_2O might be estimated from $SiH_4 + 40N_2O \rightarrow SiO_2 + 2H_2O + 36N_2O$, although this neglects the side reaction to NO.[9] We have not determined the minimum ratios of oxidant flow to SiH_4 flow necessary to produce fully oxidized film, but we know that 125 is sufficient for N_2O, 25 for NH_3, and 40 for N_2. Once gas flows have been set, F_c can be determined easily by detecting the point of Si_2H_6 disappearance as power is increased, as shown in Fig. 3(top). Here, conventional mass spectrometry with downstream leak valve sampling can be used, since Si_2H_6 is a stable gas. Notice also in Fig. 3(top) that deposition rate starts to drop off again at a power level well above F_c. We have seen this in deposition from NH_3 and from N_2O, and we believe that it is due to film material nucleating as particles within the plasma and being swept downstream. Excessive power may be dissociating film precursor molecules formed in the plasma and therefore activating their reaction with each other before they reach the surface. We will have more to say about this in Sec. III B.

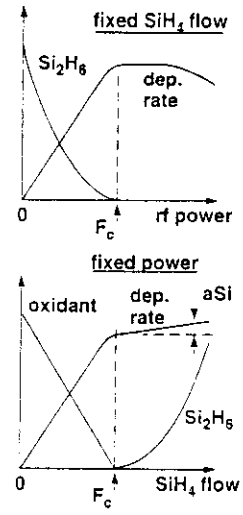

FIG. 3. Behavior of dielectric PECVD processes with plasma rf power and silane mass flow rate. F_c is the critical value of F from Eq. (1).

Figure 3(bottom) shows the complementary approach to determining F_c, in which SiH_4 flow rate is increased at a fixed power level. There, zero SiH_4 flow corresponds to a plasma of pure oxidant source gas having some level of active oxidant which is determined by the power applied. As SiH_4 flow is increased, the oxidant signal decreases linearly towards zero as it is consumed by $^{\bullet}SiH_n$, while deposition rate increases linearly. When F_c is reached, the oxidant is gone, Si_2H_6 appears, and deposition rate almost levels out. The residual slope of the deposition rate presumably represents that fraction of the excess SiH_4 which is being deposited as a-Si. This is the region of Si-rich film deposition. Again, F_c can be determined downstream using the Si_2H_6 signal. This procedure is essentially a titration for the active oxidant using SiH_4. The steep slope of the deposition rate versus SiH_4 flow in the excess-oxidant region turns out to correspond to nearly full conversion ($>50\%$) of SiH_4 to dielectric film for all three oxidants, when an approximate mass balance is calculated assuming uniform deposition on all surfaces contacting the plasma. Thus, the SiH_4 flow can be set by this calculation to produce the desired deposition rate, and then the power can be increased until excess oxidant is present. As a calibration point, in nitride deposition from NH_3 we obtained 32 nm/min for 2 sccm of SiH_4 flow in the 180 cm^2 reactor. Flow required for a given deposition rate is of course expected to scale with deposition area. There is probably an upper limit to the deposition rate of good film even if excess active oxidant can be maintained, due to problems such as gas-phase particle nucleation and film ion bombardment damage.

A. Precursor formation

The three deposition mixtures behave very differently among each other with regard to the formation of deposition precursor molecules within the plasma, and this has a profound effect on the properties of the films. Here we are referring to precursors formed in the preferred excess-oxidant regime of plasma chemistry. In this regime, none of the films have any Si–H bonding detectable by infrared absorption spectroscopy, because the Si is fully oxidized; and it is in this regime that good dielectric properties are obtained.

With NH_3,[1] essentially all of the SiH_4 is converted to tetra-aminosilane—$Si(NH_2)_4$—and the triaminosilane radical—$^{\bullet}Si(NH_2)_3$. These species adsorb on the surface with a low sticking coefficient, and there they undergo chemical condensation towards stoichiometric Si_3N_4 with the elimination of ammonia. The two overall reactions are

$$SiH_4 + 4NH_3 \rightarrow Si(NH_2)_4 + 4H_2,$$

$$3Si(NH_2)_4 \rightarrow Si_3N_4 + 8NH_3.$$

The higher the substrate temperature, the further the second reaction proceeds, although even at 450 °C, there is still 26 at. % H in the film, appearing bonded to excess N. The films have high intrinsic tensile stress which increases with deposition temperature as shown in Fig. 4, and this is likely due to the continuation of ammonia elimination beneath the surface. (Nitride films deposited under these conditions but at rf frequency below 800 kHz where ion bombardment energy is much higher have compressive stress which is believed due to compensation by the "ion peening" effect.)

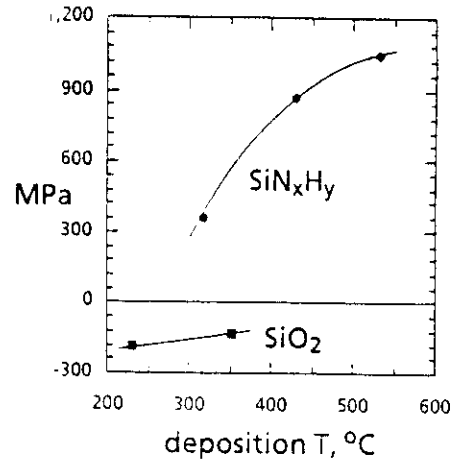

FIG. 4. Intrinsic stress of silicon nitride and oxide films.

By contrast, $SiH_4 + N_2$ plasma forms no Si–N precursors,[2] so the depositing species must be $^{\bullet}SiH_n$ and $^{\bullet}N$. Films deposited from this plasma are seen in the cross sectional transmission electron micrograph of Fig. 5 to have the classic microcolumnar "zone 1" structure which develops due to statistical roughening and self-shadowing when the depositing species have high sticking coefficients and low surface mobilities. Films deposited from NH_3 showed none of this structure and were completely homogeneous. Conformality of deposition into trenches was also poor with N_2 and good with NH_3. The stress of the films from N_2 was near zero. Low stress is expected for a loose microcolumnar structure and does not necessarily result from the deposition chemistry in this case. It is possible

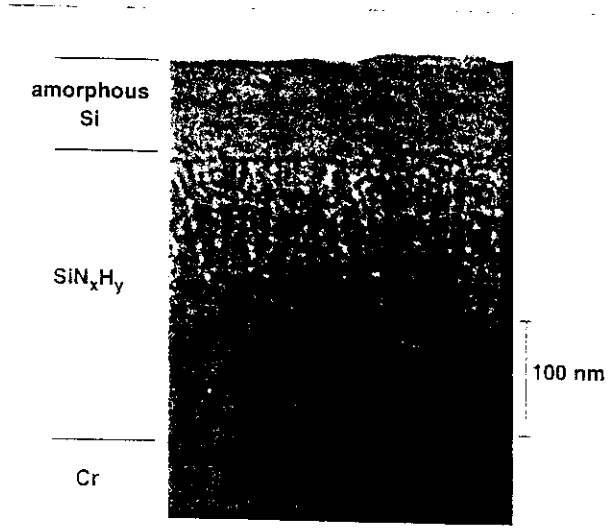

FIG. 5. Cross-sectional transmission electron micrograph (TEM) of SiN_xH_y deposited from $SiH_4 - N_2$, showing microcolumnar structure. (TEM by Greg Anderson of Xerox Palo Alto Research Center.)

that higher ion bombardment flux during deposition would be able to collapse the microvoids.

The $SiH_4 + N_2O$ plasma forms silanol molecules such as $Si(OH)_4$ which do deposit,[3] and heat is expected to drive their condensation to SiO_2 in analogy to the behavior of $Si(NH_2)_4$. Indeed, the SiO–H bond content of the SiO_2 films decreases with increasing deposition temperature. However, the stress is compressive and decreases with increasing deposition temperature, as seen in Fig. 4. This is just the opposite of the NH_3 process behavior and opposite of what is expected for film formation by chemical condensation. Therefore, it may be that these precursors are minor contributors compared to other possibilities such as SiO_n, $^{\bullet}SiH_n$, $^{\bullet}O$, or $^{\bullet}OH$. Now, the partial pressure of the $Si(OH)_4$ turned out to be proportional to the square of the partial pressure of the sum of the reactants ($SiH_4 + N_2O$), which was also the case for $Si(NH_2)_4$ in the NH_3 process. This is the expected behavior for second-order reaction kinetics, where here the two reactants are the $^{\bullet}SiH_n$ and oxidant radicals. However, when the ($SiH_4 + N_2O$) partial pressure is raised above 40 Pa or so, the deposition rate drops steadily towards zero, and particles deposit downstream. Although some particles were seen in the $SiH_4 + NH_3$ plasma too above 40 Pa (by laser light scattering), the deposition rate did not drop. This suggests that the silanols can react with each other much more readily in the gas phase than can the aminosilane, forming particles which are swept downstream. Excessive power also may be encouraging this reaction, as evidenced by the rate dropoff seen in Fig. 3(top) for both oxide and nitride. The reactant partial pressure can be reduced either by total pressure reduction or by dilution in He, Ar, or N_2; all have identical effects on $Si(OH)_4$ partial pressure, deposition rate, and film SiO–H content, which drops slightly.

Two aspects of film composition are worth noting here. In SiN_xH_y, H bonding shifts from the Si to the N as the N/Si ratio increases, as has been observed by many people. This shift is complete in the excess-oxidant regime, where N-rich films devoid of Si–H bonding are obtained, at least to the 1% sensitivity of infrared absorption. The distribution of H can be understood by considering a hypothetical amorphous Si–N network having the N/Si ratio of crystalline Si_3N_4. There will be many broken bonds in this network due to the statistical problem of the 4 bonds of each Si and the 3 bonds of each N reaching each other in a disordered network; that is, the network is overcoordinated. For the 4/3 ratio, there is one dangling N bond for every dangling Si bond. The H, having only one bond, serves the important role of terminating dangling bonds in many materials. Indeed, this is what produces the band gap in amorphous Si. In the Si–N network with N/Si = 4/3, the H will become evenly distributed as N–H and Si–H. Now, if one N atom is removed, making the network Si-rich, only Si dangling bonds are created and only Si–H is added. Conversely, for Si removal only N–H is added. The ultimate limit to N richness is the precursor molecule $Si(NH_2)_4$, which then relaxes back towards Si_3N_4 by NH_3 elimination from the film. Indeed, the ratio of excess N to total H in SiN_xH_y is the 1/3 ratio of NH_3.[1] Thus, nitride deposited in the excess-oxidant regime is saturated with NH and NH_2 groups.

The second aspect of PECVD film composition regards the amount of H, which is about an order of magnitude higher in SiN_xH_y than in SiO_2: 20 versus 2 at. %. This is likely due to the fact that the NH group, with only two bonds, is much easier to coordinate into an amorphous network than is N. Once the NH is coordinated, a third bond to Si for the N is much harder to find, so the H remains. One may think of NH in SiN_xH_y as the chemical analog of O in SiO_2; similarly, NH_2 is the analog of OH. Coordination of the amorphous network by NH may be the explanation for the superior electrical quality of N-rich nitride deposited from NH_3, which will be discussed in Sec. IV.

B. Kinetic analysis

It is useful to estimate the rates of the various plasma chemical processes in order to determine which ones will dominate under particular process conditions, such as pressure. For the most part, a molecule in the plasma will encounter one or more of the following four fates: electron-impact reaction, reaction with a free radical, reaction at the wall, or pumpout. Regarding the first two, the number of collisions per second per particle of a given particle type (electron or free radical) with any molecule is given by the particle's mean speed, c, divided by its mean free path, l; so the total collision rate of those particles per unit volume ($cm^{-3}\,s^{-1}$) is c/l times the particle concentration, n_e or n_r (cm^{-3}), respectively. Now, the rate r_i (s^{-1}) at which an individual molecule in the plasma encounters a collision with a particle of type i is given by the collision rate of i per unit volume divided by the total molecular concentration, n (cm^{-3}). Thus,

$$r_i = \frac{c_i}{l_i}\frac{n_i}{n}. \tag{2}$$

We will now estimate the quantities to use in this equation. Parallel-plate glow discharge plasmas typically have a "plasma density" of $n_e \approx 10^{10}$ electrons (or ions) per cm^3. (More sophisticated plasma generators, employing electron cyclotron resonance, helicon waves, or inductive coupling, can have much higher densities of $\approx 10^{12}$ cm^{-3}). Plasma density is determined mainly by power input and is not a strong function of pressure. Also, the parallel-plate discharge typically has an electron "temperature" (though non-Maxwellian) of a few eV. But higher energy than that is required to dissociate a molecule (8 eV for SiH_4), so let us say that 10% of the electrons in the energy distribution have the required energy. It is the density of these fast electrons, $n_e \approx 10^9$ cm^{-3}, that determines the electron-impact reaction rate. The speed of an 8 eV electron is $c_e = 2\times 10^8$ cm/s. Finally, l_e is determined roughly by the molecular cross section, σ_m, in this energy range; that is, $l_e = 1/\sigma_m n = 4/\pi a^2 n$, where a is the molecular diameter, ≈ 0.3 nm. Combining all these quantities into Eq. (2), we see that n cancels and that $r_e = 140\ s^{-1}$, which is indepen-

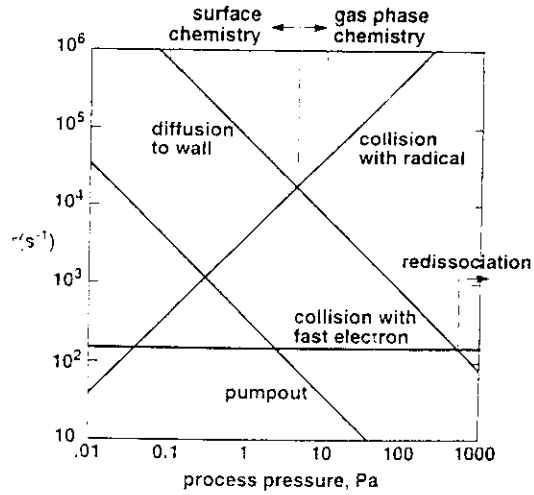

FIG. 6. Approximate rates per molecule of various events which a molecule can encounter in a glow-discharge plasma. Conditions and assumptions are given in the text.

dent of pressure. This is the electron-impact reaction rate per molecule; the reaction rate per unit volume is then $r_e n$ ($cm^{-3}\,s^{-1}$).

The same calculation can be done for free radicals. Here, the collision cross section is roughly twice σ_m, and a $\sqrt{2}$ factor is added to account for the motion of the two particles towards each other at an average angle of 90°, so that $l_r = 1/\sqrt{2}\pi a^2 n$, which is a factor of 6 less than l_e. At 25 °C, mass 40 Maxwellian particles have $c = 4\times10^4$ cm/s, and ideal gas has $n = 2.4\times10^{14}p$ cm^{-3} (p in Pa). For the free radical concentration, n_r, we will take as a typical value 10% of n. This fraction will increase with plasma power and decrease with increasing mass flow rate, but it is not expected to be a strong function of pressure. This is because diffusion loss to the walls decreases with increasing p, but dilution in n increases with p. Combining these factors into Eq. (2), we find that r_r (s^{-1}) = 3840p (Pa). Both r_e and r_r are plotted versus p in Fig. 6.

The third fate of a molecule is reaction at the wall. The upper limit of this reaction rate is the diffusion rate to the wall. The diffusion length over a time τ is given by $\Lambda = 2\sqrt{D\tau}$, so the rate at which an individual molecule reaches the wall is $r_d = 1/\tau = 4D/\Lambda^2$. Taking $\Lambda = 1$ cm and D (cm^2/s) = $2\times10^4/p$ (Pa) for 25 °C Ar, we have r_d (s^{-1}) = $8\times10^4/p$ (Pa). Finally, the pumpout rate per molecule is the inverse of the residence time, or $r_p = W/V$, where W is the volume flow rate and V is the plasma volume. A typical mass flow rate of 100 sccm gives W (cm^3/s) = $1.8\times10^5/p$ (Pa) at 25 °C, and our 15 cm diam plasma with 3 cm electrode spacing has $V = 530$ cm^3. Thus, r_p (s^{-1}) = 340/p (Pa). Both r_d and r_p are also plotted versus p in Fig. 6.

Comparison of these four order-of-magnitude rate estimates and their pressure dependence in Fig. 6 helps in understanding the behavior of the dielectric film deposition processes discussed above. Consider the species $^{\bullet}SiH_n$ undergoing these four processes. It has already undergone electron-impact dissociation in its creation, and we want to know what happens to it next. In the 100 Pa range of conventional rf PECVD, Fig. 6 shows that it is going to undergo almost 10^3 collisions with other (oxidant) radicals before the next electron impact. These collisions will mostly be reactive ones, since the activation energy of radical–radical reactions is zero. This high reaction rate explains how such a complicated molecule as $Si(NH_2)_4$ can be created in the high-energy environment of a plasma, and also why the array of species created is not more complex. Thermochemically driven reactions between radicals are dominating the plasma chemistry, so the products are going to be selectively those of low free energy.

These products—the deposition precursors—must next diffuse to the wall or substrate. The diffusion rate decreases with increasing pressure, and for pressures above 600 Pa or so, Fig. 6 shows that redissociation by a second electron impact becomes the more likely event. The crossover pressure would be lower at higher plasma power because of a higher fast-electron collision rate. This may be the explanation for the deposition rate decrease and particle formation at high reactant pressure or high power, because redissociated precursors would be more reactive with each other in the gas phase. Even without redissociation, they have more time to react at higher pressure before diffusing to the wall and depositing.

Going down in pressure from the 100 Pa range, other crossovers are reached. Below 5 Pa, diffusion to the wall becomes faster than radical reaction, so precursors will not form in the gas phase. Instead, all of the film-forming reactions will occur on the surface and will involve the primary radicals produced by electron impact. The requirement of excess oxidant for dielectric deposition would remain important, but gas-phase precursors such as $Si(NH_2)_4$ and $Si(OH)_4$ would not be involved as intermediates. At still lower pressure, the feed gas is pumped out before electron impact reaction can occur, so reactant utilization decreases. This crossover pressure will be lower for the higher plasma densities available from other types of generators, because there the electron collision rate is higher.

IV. FILM ELECTRICAL PROPERTIES

When the F given by Eq. (1) is high enough so that the deposition process is operating in the excess-oxidant regime, dielectric films are obtained from either NH_3 or N_2O which have low-leakage I–V characteristics and narrow ramp breakdown ranges.[3,4] To more finely distinguish among such films and to compare them with similarly behaving films made by other processes, avalanche injection has been used to measure the electron trapping rate in the bulk of the films.[5,6,10] Its application to these films has been desribed in detail elsewhere,[10] but the basic idea is illustrated in Fig. 7. The film is deposited onto a p-doped crystalline Si wafer which has been thermally oxidized to minimize interfacial trap state density. After front and back metallization, the flatband voltage V_{fb} of this metal–insulator–semiconductor (MIS) structure is determined from the capacitance–voltage (C–V) curve. Then, a negative voltage pulse is applied to the Si, causing avalanche

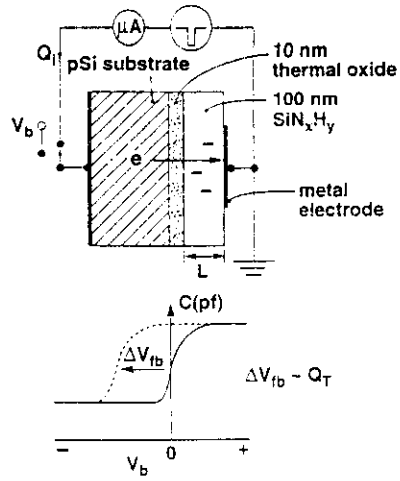

FIG. 7. Avalanche injection measurement of electron trapping in a dielectric film such as SiN_xH_y: MIS capacitor structure and measurement circuit (top); C–V_b curve and the V_{fb} shift due to negative charge Q_T trapped in the dielectric film (bottom).

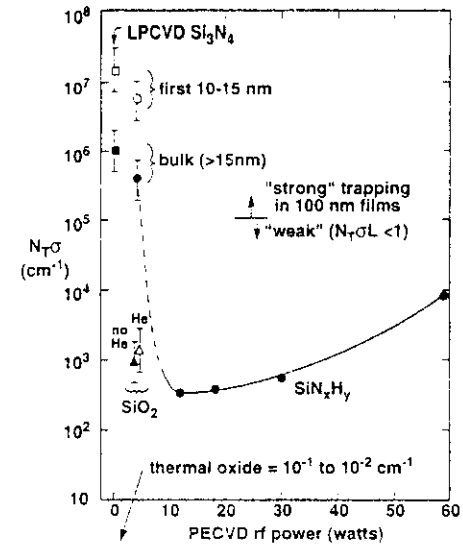

FIG. 8. Trapping coefficient, $N_T\sigma$, for various nitride and oxide films as measured by avalanche injection. Those films plotted at rf power >0 were deposited by PECVD, all in the reactor described in Sec. II.

injection of a measured charge of electrons Q_i into the dielectric. The amount of charge trapped Q_T is found from the negative shift which its presence in the dielectric produces in the C–V curve. If part of the injected charge passes through to the metal electrode before being trapped, the fraction trapped is given by

$$Q_T/Q_i = (N_T\sigma)L \tag{3}$$

where N_T (cm^{-3}) is the trap density in the deposited dielectric film, σ (cm^2) is the trapping cross section, and L (cm) is the film thickness. $N_T\sigma$ (cm^{-1}) is essentially an absorption coefficient or trapping coefficient for electrons per unit thickness of film. If, on the other hand, $(N_T\sigma)L$ is so large that all of the injected charge becomes trapped, then the depth to which the charge penetrates into the film, $L_T(<L)$, must be determined in order to find $N_T\sigma$. This too can be determined from the C–V shift.[10] The former situation ($N_T\sigma L<1$) is known as weak trapping and the latter as strong trapping. In strong trapping, the film is essentially "electron-opaque."

The quantity $N_T\sigma$ has been calculated from avalanche measurements reported previously on various oxide and nitride films,[5,6,10] and these values are plotted in Fig. 8. Separate determination of N_T and σ will require more measurements, but for all but the thermal oxide, N_T was estimated to be on the order of 10^{18} cm^{-3}. Figure 8 shows an enormous range of 10^9 in $N_T\sigma$ from silicon nitride deposited by low-pressure thermal chemical vapor deposition (LPCVD) to thermally oxidized Si. The PECVD films shown were all deposited in the reactor described in Sec. II, and their $N_T\sigma$ are plotted versus plasma power in that reactor. Except for the nitride film deposited at 4 W, all of these nitride and oxide films were deposited under excess-oxidant conditions ($F>F_c$). The 4 W nitride had a N/Si ratio of about 4/3, rather than being N-rich like the other nitrides, and it had H bonded to both Si and N. In this film and in the LPCVD nitride only, the first 10–15 nm deposited was found to have a higher trapping rate than the remainder of the film. In both of these films, $N_T\sigma$ is very high. Nitride deposition in the higher-power, excess $^{\bullet}NH_n$ regime is seen to reduce $N_T\sigma$ by 10^3 to a value even lower than that of the best obtainable PECVD SiO_2. The lowest $N_T\sigma$ occurs at a power just over the amount required to reach F_c, and then $N_T\sigma$ rises with additional power, possibly due to ion bombardment damage. These results show that the high trapping rate traditionally associated with silicon nitride film can be avoided by careful tuning of deposition conditions based on an understanding of the plasma chemistry. The much higher $N_T\sigma$ for the other nitrides is due largely to an increase in σ rather than in N_T.[5] Although the structural feature responsible for the high σ has not been identified, the behavior with deposition conditions points to dangling Si bonds. LPCVD nitride, which contains only a few at. % H, is likely to contain many dangling bonds because of overconstraint of the Si–N network. The PECVD nitride may not be so overconstrained, because of the flexibility of NH bonding to Si which was discussed earlier, thus allowing it to achieve an $N_T\sigma$ comparable to that of oxide. However, the 4 W PECVD nitride may be developing Si dangling bonds by diffusion of H away from Si–H bonds broken by the impact of injected electrons. Much more study is needed to clarify this situation, but it is clear that nitride deposition from NH_3 in the excess-oxidant regime results in a dramatic reduction in $N_T\sigma$.

The PECVD SiO_2 was deposited both with and without a high dilution of He,[3] and the resulting values of $N_T\sigma$ shown in Fig. 8 are the same within the accuracy of the measurement. This is consistent with our inability to detect any effect of He on the plasma chemistry, and we therefore conclude that He has no effect on the *bulk* properties of the oxide. There may be an effect of He on *interfacial* trap density, but we specifically sought to avoid interfacial effects in this work in order to study the bulk material. We

calculated the F for films deposited in the original report of the He-diluted process,[11] and found that the films having leaky I–V characteristics had low F as well as having no He in the plasma.[3] We attribute the poor electrical behavior to the low F rather than to the lack of He.

V. CONCLUSIONS

Much information about the PECVD process can be obtained by coupling plasma and film analysis. For silicon nitride and oxide films, good dielecric properties and high silane utilization are obtained when oxidant gas flow and plasma power are both sufficient to maintain an excess of oxidant radicals: that is, more than the amount needed to consume all of the silane. The deposition rate and the required power both scale with silane flow rate. After setting silane flow to obtain the desired deposition rate, the required power can be determined by observing the disappearance of the byproduct disilane, Si_2H_6, in the plasma or downstream.

In the 100 Pa range of conventional PECVD, radical–radical reaction rates are orders of magnitude faster than electron-impact dissociation rates, so that thermochemistry determines the plasma composition. If reactant pressure or rf power is too high, gas-phase particle formation and deposition rate loss develop due to excessive gas-phase reaction. At much lower pressure, reactions are expected to shift from the gas phase to the surface.

When nitride is deposited using NH_3 rather than N_2 and when the process is operated in the excess-oxidant regime, films can be obtained which have electron trapping rates at least as low as those achievable in PECVD oxide, and this may be due to the ability of NH groups to coordinate the bonding of the amorphous network as O can in oxide. He dilution in oxide deposition was found to have no effect on either plasma chemistry or electron trapping rate.

ACKNOWLEDGMENTS

Thanks go to Greg Anderson for the TEM micrograph and to Warren Jackson for discussions on charge trapping.

[1]D. L. Smith, A. S. Alimonda, C-C. Chen, S. E. Ready, and B. Wacker, J. Electrochem. Soc. **137**, 614 (1990).
[2]D. L. Smith, A. S. Alimonda, and F. J. von Preissig, J. Vac. Sci. Technol. B **8**, 551 (1990).
[3]D. L. Smith and A. S. Alimonda, J. Electrochem. Soc. (in press).
[4]D. L. Smith, A. S. Alimonda, C-C. Chen, and H. C. Tuan, J. Electron. Mater. **19**, 19 (1990).
[5]Y. C. Park, W. B. Jackson, D. L. Smith, and N. M. Johnson, J. Appl. Phys. **74**, 381 (1993).
[6]Y. C. Park, N. M. Johnson, W. B. Jackson, K. S. Stevens, and D. L. Smith, Appl. Phys. Lett. **60**, 695 (1992).
[7]A. A. Bright, J. Vac. Sci. Technol. A **9**, 1088 (1991).
[8]R. D. Levin and S. G. Lias, Natl. Stand. Ref. Data Ser., Natl. Bur. Stand. (U.S.) **71** (1982).
[9]T. A. Cleland and D. W. Hess, J. Electrochem. Soc. **136**, 3103 (1989).
[10]Y. C. Park, W. B. Jackson, N. M. Johnson, and S. B. Hagstrom, J. Appl. Phys. **68**, 5212 (1990).
[11]J. Batey and E. Tierney, J. Appl. Phys. **60**, 3136 (1986).